ChemComm

ROYAL SOCIETY OF CHEMISTRY

COMMUNICATION

View Article Online
View Journal

Cite this: DOI: 10.1039/d2cc01515c

Received 16th March 2022,
Accepted 18th July 2022

DOI: 10.1039/d2cc01515c

rsc.li/chemcomm

A unique water soluble probe for measuring the cardiac marker homocysteine and its clinical validation†

Snehasish Debnath,[ab] Ratish R. Nair,[ab] Riya Ghosh,[ab] Gaddam Kiranmai,[c] Narsini Radhakishan,[d] Narayana Nagesh *[c] and Pabitra B. Chatterjee *[ab]

A series of copper(II) compounds 1–4 were synthesized and developed as fluorogenic probes to measure the cardiac marker homocysteine (Hcy) without any interference from other bioanalytes prevalent in human blood plasma including, cysteine and glutathione. UV-vis and EPR studies have provided confirmatory evidence for reduction-induced-emission-enhancement of the probe, which is responsible for the observed "off-to-on" behaviour towards Hcy. Water solubility, remarkable fluorescence enhancement (55–111 fold), and low detection ability (nearly 2.5 μM) make the probe suitable for clinical testing of cardiac samples. Investigation of 1 against a few reductive interferents testifies its specificity for Hcy. Results from clinical examination of cardiac samples by 1 when combined with the outcome of the reliability testing involving a clinically approved commercial immunoassay kit, validates the prospect of the molecular probe for direct measurement of Hcy in human plasma, which is unprecedented.

High concentrations (>15 μM) of the cardiac marker homocysteine (Hcy, Scheme S1, ESI†) in human plasma are accompanied by the early onset of several critical health illnesses and age related pathologies *viz.* atherosclerosis and thrombosis, acute coronary heart disease, ischemic stroke, early pregnancy loss, chronic renal dysfunction, microalbuminuria, cognitive impairment, Alzheimer's disease, and Parkinson's disease.[1] Consequently, measurement of plasma total homocysteine (tHcy) is obligatory for clinical supervision of various pathologies. Despite tens of thousands of publications in the literature on the relationship between Hcy and above-mentioned health disorders, very few Hcy selective optical probes exist in the literature.[2] Ever since Strongin *et al.* reported the optical method for selective detection of Hcy,[2a] not many reports are documented in the literature describing interference-free optical detection of Hcy (Table S1, ESI†). As clearly pointed out by Strongin and co-workers,[3] the obligatory requirement of non-aqueous media for the detection purpose has presumably made the clinical application of the Hcy-specific optical probes challenging. Wang *et al.* have recently developed a BODIPY-based complex for selective detection of Hcy in an aqueous medium.[2e] However, synthetic difficulty, cost of the reagents (*i.e.* BODIPY), and lack of detailed clinical validation and testing could be a major limitation in the development of optical assays using Wang's probe.[2e]

In this communication, we report the synthesis and characterization of four water-soluble (100% aqueous) copper compounds (**1–4**) to develop optical probes for measuring Hcy directly and selectively, in clinical samples. Upon addition of Hcy, non-fluorescent **1–4** showed 55–111 fold emission enhancement at physiological pH conditions, without any interference. Mechanistic studies have provided evidence for the preferential affinity of **1–4** towards Hcy. Herein, we demonstrate clinical testing of the Hcy-specific optical probe in a large number of human samples (cardiac patients and healthy volunteers as well). The performance of our presented assay has also been tested with a clinically approved immunoassay kit involving 60 clinical samples, which is unprecedented in the literature.

Yellow solids of the ligands HL_1–HL_4 were prepared from 7-hydroxycoumarin, as described in Scheme S2 (ESI†). The purity and molecular structures of HL_1–HL_4 and copper complexes (**1–4**) were established by C/H/N, IR, NMR, and ESI-MS (Fig. S1–S17, ESI†). Structural confirmation was gained from single crystal X-ray analyses (Fig. 1a and Fig. S13, Tables S2 and S3, ESI†). The structural index parameter τ (= 0.07), determined from the equation $\tau = (\beta - \alpha)/60$ (wherein, β and α are the two largest *L*–M–*L* angles),[4] indicates the square pyramidal geometry of the copper complex. Water-soluble 1–4 showed two weak absorption peaks as shoulders at 410 and 365 nm (Fig. S18, ESI†).

[a] *Analytical & Environmental Science Division and Centralized Instrument Facility, CSIR-CSMCRI, G. B. Marg, Bhavnagar, Gujarat, India. E-mail: pbchatterjee@csmcri.res.in*
[b] *Academy of Scientific and Innovative Research (AcSIR), Ghaziabad 201002, India*
[c] *Medical Biotechnology Complex, CSIR-CCMB, ANNEXE II, Hyderabad, Telangana, India. E-mail: nagesh@ccmb.res.in*
[d] *Department of Biochemistry, Nizam's Institute of Medical Sciences, Punjagutta, Hyderabad, Telangana, India*

† Electronic supplementary information (ESI) available: Materials and methods, synthesis, characterization data, Fig. S1–S53, Schemes S1–S3 and Tables S1–S7. CCDC 2105918–2105921. For ESI and crystallographic data in CIF or other electronic format see DOI: https://doi.org/10.1039/d2cc01515c

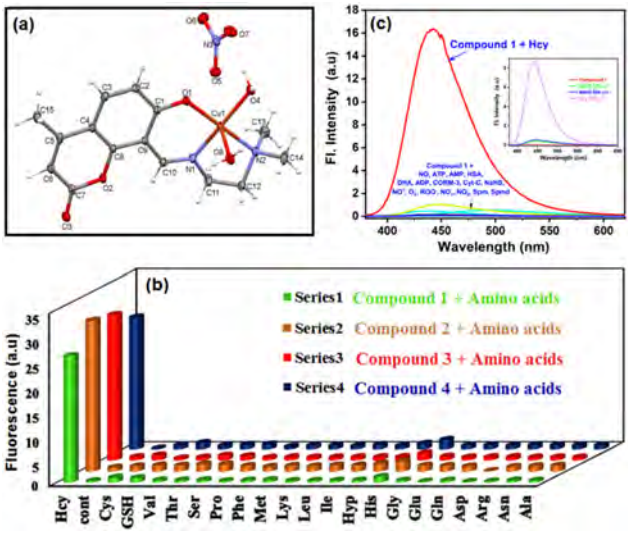

Fig. 1 (a) ORTEP view and atom-numbering scheme of the copper compound 1. (b) Fluorimetric responses of **1–4** (20 μM) toward different amino acids upon excitation at 370 nm in aqueous HEPES buffer solution (10 mM) at physiological pH (7.4). (c) Fluorescence responses of **1** (20 μM) towards other biologically relevant species (125 μM). Inset: Fluorescence of **1** (20 μM) towards variable concentrations of NaHS.

Furthermore, the complex displayed a d–d band at 625 nm (ε, 160 L mol^{-1} cm^{-1}). Because of the unique physical properties, high quantum yield, and great binding ability towards various analytes, coumarin derivatives have been found as fantastic fluorophores in the literature.[5] As a result of C=N isomerisation and/or electron transfer processes,[6] HL_1–HL_4 are weakly fluorescent (Φ_f = 0.01–0.014). However, complexes **1–4** are non-luminescent. The high binding affinity of Cu^{2+} towards ONN donor sites of HL_1–HL_4 further restricts the hydrolysis of 1–4 at neutral pH,[7] which has been confirmed from the pH profile (*vide infra*).

Emission behaviour of **1–4** against different amino acids is shown in Fig. 1b and Fig. S19 (ESI†), which revealed a large luminescence enhancement upon addition of Hcy with the formation of cyan colour (Fig. S20, ESI†). To check the efficacy of the probes for clinical applications, pH-variable luminescence measurement of **1–4** was explored further (Fig. S21–S24, ESI†). Throughout the pH regime, **1–4** remained non-fluorescent. To our surprise, emission spectra of **1–4** with Hcy showed maximum fluorescence at physiological pH. Hence, the working pH was found to be 6.5–8 (Fig. S21–S24, ESI†). All spectral experiments were performed with aqueous HEPES buffer (100% water) at physiological pH. We further have investigated the time-response behaviour of **1** in presence of Hcy. Results shown in Fig. S25 (ESI†), discloses that the luminescence intensity of **1** reaches a maximum within 60–70 min incubation with Hcy. Cys initially shows a little turn-on response. However, after 7–8 min incubation, the solution turned non-fluorescent. Luminescence spectra of **1–4** were measured after incubation of the probes with various amino acids and GSH for 30 min. A sharp 55–111 fold fluorescence increase was observed with Hcy. Thus, demonstrating Hcy selective nature of **1–4**. The quantum yields were estimated to be within 0.134 to 0.091, much higher than the ligands. Thus, indicating adduct formation between Hcy and probes, instead of the replacement of the iminocoumarin ligand from the probes. From the Job's plot, the binding stoichiometry was found to be 1 : 1 (Fig. S26, ESI†). Without any interference, **1–4** responded to Hcy, even in presence of Cys and GSH (Fig. S27–S30, ESI†). Interference of Hcy congeners, *i.e.* Cys and GSH, have also been tested in different stoichiometric mixtures of them with Hcy. Results displayed in Fig. S31 (ESI†) reveals non-interference from Cys and GSH during the detection of Hcy. From fluorescence titration (Fig. S32–S35, ESI†), the calculated binding constants were found to be in the range 1.23–2.15 × 10^3 M^{-1} (Fig. S36, ESI†). The limit of detection (LOD) was calculated (Fig. S37, ESI†) to be in the order of 2.5 μM (compound **2**), which is below the normal level of Hcy in healthy human blood plasma. Linearity within 0–100 μM supports the suitability of **1–4** at low concentration. Remarkable specificity of the probe towards Hcy is further reinforced when **1** was screened against a range of important bioanalytes (Fig. 1c). Furthermore, using varying concentrations of NaHS and other sulfur containing interferents that are commonly present in blood plasma, the non-emissive nature of the probe did not change (inset, Fig. 1c and Fig. S38, ESI†).

Reversible detection of Hcy by the probes (Fig. S39, ESI†) clearly demonstrates that the displacement of the ligand by the incoming Hcy ligand is not happening in **1–4**. Thus, not in line to the proposal of Kim *et al.*[7] This could be the result of the redox reaction between probe and Hcy, wherein, Hcy reduces Cu(II) to Cu(I) at physiological pH. Upon deprotonation, Hcy binds Cu(I). Therefore, a ternary Cu(I) complex is formed. ESI-MS of **1**, when recorded after half an hour of incubation with Hcy, showed a molecular ion peak of the intermediate ternary species at m/z = 512.58. This clearly implies the formation of the intermediate Cu(I) species, as shown in Fig. S40 (ESI†). Presumably, the reduction of Cu(II) is responsible for the fluorimetric "off-to-on" responses of **1–4** with Hcy. On the contrary, Cys with one less methylene group (Scheme S1, ESI†), initially showed a turn on response, which quickly diminished over time. After 7–8 min incubation, the solution mixture quenched completely. The pK_a value of the sulfhydryl group of Cys (8.00) is lower than that of Hcy (8.87).[8] As a result, Cys deprotonates faster than Hcy at physiological pH and it exists predominantly in the thiolate form. The isoelectric points of Hcy and Cys are 5.65 and 5.02, respectively.[9] Hence, both Hcy and Cys exist as negatively charged species at physiological pH. With Cu(II), Cys reacts faster than Hcy, resulting in the formation of a kinetically unstable 5-membered ring (as shown in Scheme S3, ESI†). The sulfhydryl group of Hcy deprotonates at a relatively slower rate than Cys. The deprotonated Hcy undergoes complexation with Cu(II) to form a kinetically favoured six membered ring. In both cases, a distinct fluorescence was initially observed upon addition of Hcy or Cys to the aqueous solutions of **1–4**. This could be presumably due to the reduction of Cu(II) to Cu(I), which subsequently disrupts the PET process causing restoration of the fluorescence intensity. Interestingly, the fluorescence intensity of the probe was dramatically quenched for Cys after 8 min incubation. Whereas, it reaches a plateau after 60 min incubation with Hcy (Fig. S25, ESI†). In case of Cys, the

unstable five membered ring is not kinetically favoured. Hence, following the decomplexation of Cys, Cu(I) quickly gets oxidized to Cu(II) by the dissolved oxygen in the medium.[10]

The electronic spectrum of **1** (Fig. 2a) displays a d–d band at 625 nm.[11] Upon addition of Hcy, the band disappeared suggesting the formation of Cu(I) species. Supplementary experimental evidence in support of the above mentioned redox mechanism is also revealed from EPR studies. As expected, in the absence of Hcy, **1** displayed a 4-line EPR spectrum with g values, $g_{\parallel}$ = 2.141 and $g_{\perp}$ = 2.044.[12] On addition of Hcy to **1**, EPR of the mixture turned silent (Fig. 2b). Clearly, the reduction of Cu(II) with Hcy is supported by EPR. Time dependent fluorescence of **1** with variable concentrations of Hcy/Cys was further explored to support the mechanism. Separate kinetic investigations of **1** with Hcy and Cys were performed at 7.4 pH. Following pseudo first order kinetics, the change in fluorescence intensity has been fitted against time following the equation mentioned in the literature.[13] Initial kinetic data of **1** (20 μM) with 500 μM Hcy/Cys is shown in Fig. S25 and S41 (ESI†). The observed rate constants (k_{obs}) are 0.039 and 1.73 min^{-1} for Hcy and Cys, respectively (Fig. S41–S43, ESI†). Clearly, the k_{obs} values hint at a faster reaction rate of Cys than Hcy, as already revealed in the earlier section. Interestingly, the short half-life ($t_{1/2}$) of Cys (0.40 min) further confirms the instability of the five membered ternary intermediate compared to the six membered conjugate with Hcy (**1**-Hcy adduct, $t_{1/2}$ = 17.77 min). The kinetic profile of **1** towards variable concentrations of Hcy was examined next (Fig. S42, ESI†). The observed rate constant (k_{obs}) values were calculated to be 0.039, 0.043, 0.082, and 0.204 min^{-1} for 500, 250, 100, and 50 μM Hcy, respectively (Fig. S43, ESI†). The $t_{1/2}$ values for 500, 250, 100 and 50 μM Hcy were found to be 17.77, 16.11, 8.45, and 3.4 min, respectively. The increase in the half-life value with a rise in the Hcy concentration undoubtedly confirms the kinetic stability of the intermediate at a higher concentration regime.

Finally, time correlated single photon counting (Fig. S44–S47, ESI†) showed a decrease in the fluorescence lifetime (τ) of **1** from 5.58 ns to 5.15 ns upon addition of Hcy (Table S5, ESI†). Radiative (k_r) and total non-radiative (k_{nr}) rate constants are given in Table S5 (ESI†). Higher k_{nr} values of **1–4** (Table S5, ESI†) presumably refer to the photoexcited electron transfer (PET) processes occurring in **1–4**.[14] This event has ultimately resulted in the low k_r values, which is reflected in the observed non-emissive nature of **1–4**. From Table S5 (ESI†), it is clear that the key factor for fluorescence enhancement of **1–4** with Hcy is k_r. Therefore, addition of Hcy to the probe's solution has resulted in the drop of the non-radiative deactivation pathway (*i.e.* quenching of the PET process).[14] As discussed earlier, binding of Hcy to Cu(II) reduces the metal center, which ultimately inhibits the PET process causing fluorescence enhancement of the probes with Hcy. In other words, reduction-induced-fluorescence-enhancement of the probes has resulted in the development of an optical method for the direct measurement of Hcy in aqueous samples.

Surprisingly, Hcy selective probes reported hitherto in the literature are not water-soluble. Table S1 (ESI†) seems to suggest that Hcy specific organic probes are hydrophobic in nature. However, metal complex derived probes are ionic, as described in this work and earlier by Li *et al.* Therefore, the ionic complexes would be a good choice for developing water-soluble probes.[2e] Validation and clinical testing of the probes are two key studies that are indispensable to ascertain the usability and prospects of the developed optical probes for biomedical research. Observation from Table S1 (ESI†) reveals that researchers have under-investigated this aspect while developing Hcy-specific probes. Herein, we sought to validate 1 with the HPLC method first. For this purpose, different concentrations of Hcy were derivatized with thiol selective UV labelling reagent.[15] A linear calibration plot (ranging 5–100 μM) was generated by plotting the ratio of peak area of Hcy to internal standard (IS) *versus* concentration of injected Hcy (Fig. 3a). A few representative chromatograms are shown in Fig. S48 and S49 (ESI†). To validate our assay, two unknown concentrations of Hcy were prepared from 100 μM stock solution. The concentrations of the unknown Hcy solutions were then measured by the fluorescence technique (Fig. 3b) using **1** as well as by the HPLC method (Fig. 3a). The experimentally measured values by both the techniques compare considerably with an error percentage of 2 (Table S6, ESI†). Hence, the results validates the optical sensor reported in this work.

To carry out the real-world application of **1** for early diagnostic drive, we tested **1** for direct measurement of Hcy in the blood plasma of a good number of cardiac patients. Retention of the 4 line EPR of **1** for more than half a day indicates the stability of the probe in blood plasma (Fig. S50, ESI†). Kinetic experiments were also performed in blood plasma (Fig. S51, ESI†). It reveals fluorescence regeneration of **1** on addition of Hcy to the quenched plasma sample. This implies the non-displacement of the Cu ion from iminocoumarin ligand even in blood plasma.

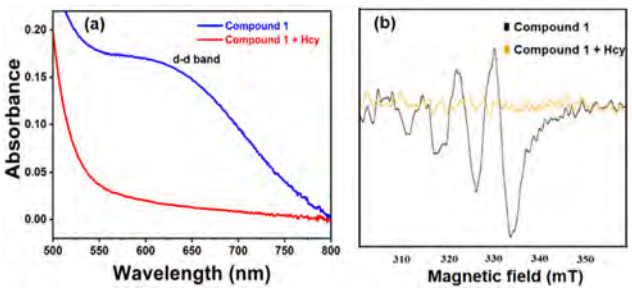

Fig. 2 (a) UV-vis spectra of **1** in the presence (blue line) and absence (red line) of Hcy (1 mM) in aqueous solution. (b) EPR spectra of **1** in the presence (black line) and absence (yellow line) of Hcy in an aqueous solution.

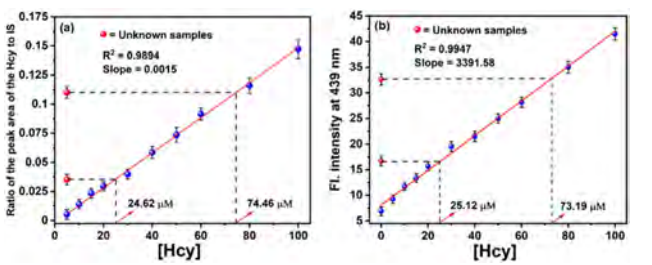

Fig. 3 Measurements of unknown concentrations of Hcy (a) using HPLC technique and (b) utilizing the linear fluorimetric calibration curve of **1** with Hcy in HEPES buffer solution (10 mM, pH = 7.4).

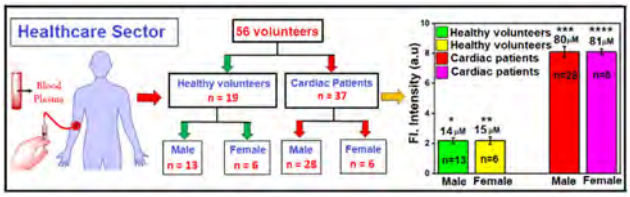

Fig. 4 Schematic representation showing Hcy levels measured by **1** in the blood samples of cardiac patients and healthy volunteers. In all cases (*, **, ***, and ****) $P < 0.05$. Each data point represents the average of triplicates.

Results from cytotoxicity studies of **1** and related Cu(I) species suggested no obvious toxicity (Fig. S52, ESI†). We next undertook the unique challenge of clinical investigation of **1**, which could be a potential candidate for point-of-care use. As expected, the fluorescence intensity of **1** was significantly lower in healthy volunteers than cardiac patients (Fig. 4). The total Hcy levels measured in the healthy volunteers were found to be in the range 09–17 μM and 10–16 μM in male and female categories, respectively. Meanwhile, the plasma tHcy levels in cardiac patients were calculated to be 70–82 μM and 74–80 μM in male and female samples, respectively (Fig. 4). The data presented in Fig. 4 indicates that the cardiac patients studied in this work have been suffering from intermediate hyperhomocysteinemia. Unprecedented clinical validation of our presented optical probe has also been performed by comparing the Hcy levels in a large number (sixty) of clinical samples. A clinically approved commercial immunoassay kit and current optical assay have been used to measure plasma tHcy levels in clinical samples. The results shown in Fig. S53 and Table S7 (ESI†) indicate that the Hcy level measured by the probe **1** compares reasonably well with the commercial kit. Thus, a simple and straightforward assay has been established in this work, which paves the way towards the possibility of the development of a miniature POCT kit for routine analysis and prognosis of various critical illnesses connected to HHcy in low resource settings.

In summary, we have reported herein a series of water soluble optical probes, which displayed a highly selective and interference-free turn-on fluorescence response towards homocysteine. EPR and UV-vis investigations provided evidence for the reduction-induced-emission-enhancement of the probes with Hcy. Validation of the presented optical assay has been performed by the traditional HPLC technique and reliability testing of **1** with regard to the clinically approved commercial immunoassay kit involving a large number of human plasma samples validates the simplicity and real-world application prospects of **1** as a novel molecular probe to measure the cardiac marker Hcy in patients' blood samples. Optical measurement of Hcy in human plasma samples using **1** and demonstration of its validation with sixty clinical samples is the first of its kind. The chemicals for preparing the probe and reagents required for the assay are inexpensive. Therefore, the present method reported herein demonstrates the feasibility for the development of a Hcy-selective diagnostic kit to be suitable for point-of-care testing.

This work is supported by the Govt. of India through the CSIR Grant no. MLP0047 and SERB (Grant no. CRG/2020/000577). SD and RRR acknowledge CSIR for their SRFs. The manuscript has CSIR-CSMCRI registration number 161/2021. Prior consent was obtained from human subjects.

Conflicts of interest

The authors declare no conflict of interest.

Notes and references

1 (*a*) G. E. Lonn, S. Yusuf, M. J. Arnold, P. Sheridan, J. Pogue, M. Micks, J. Probstfield, G. Fodor, C. Held and J. J. Genest, *N. Engl. J. Med.*, 2006, **354**, 1567–1577; (*b*) S. Seshadri, A. Beiser, J. Selhub, P. F. Jacques, I. H. Rosenberg, R. B. D'Agostino, P. W. F. Wilson and P. A. Wolf, *N. Engl. J. Med.*, 2002, **346**, 476–483; (*c*) H. Refsum and P. M. Ueland, *Annu. Rev. Med.*, 1998, **49**, 31–62; (*d*) M. Sibrian-Vazquez, J. O. Escobedo, S. Lim, G. K. Samoei and R. M. Strongin, *Proc. Natl. Acad. Sci. U. S. A.*, 2010, **107**, 551–554.
2 (*a*) W. Wang, J. O. Escobedo, C. M. Lawrence and R. M. Strongin, *J. Am. Chem. Soc.*, 2004, **126**, 3400–3401; (*b*) X. Yang, Y. Guo and R. M. Strongin, *Angew. Chem., Int. Ed.*, 2011, **50**, 10690–10693; (*c*) H. Peng, K. Wang, C. Dai, S. Williamson and B. Wang, *Chem. Commun.*, 2014, **50**, 13668–13671; (*d*) H. Y. Lee, Y. P. Choi, S. Kim, T. Yoon, Z. Guo, S. Lee, K. M. K. Swamy, G. Kim, J. Y. Lee, I. Shin and J. Yoon, *Chem. Commun.*, 2014, **50**, 6967–6969; (*e*) Z. Li, Z. R. Geng, C. Zhang, X. B. Wang and Z. L. Wang, *Biosens. Bioelectron.*, 2015, **72**, 1–9; (*f*) J. Wang, Y. Liu, M. Jiang, Y. Li, L. Xia and P. Wu, *Chem. Commun.*, 2018, **54**, 1004–1007; (*g*) J. O. Escobedo, W. Wang and R. M. Strongin, *Nat. Protoc.*, 2007, **1**, 2759–2762.
3 C. X. Yin, K. M. Xiong, F. J. Huo, J. C. Salamanca and R. M. Strongin, *Angew. Chem., Int. Ed.*, 2017, **56**, 13188–13198.
4 R. R. Nair, M. Raju, K. Jana, D. Mondal, E. Suresh, B. Ganguly and P. B. Chatterjee, *Chem. – Eur. J.*, 2018, **24**, 10721–10731.
5 D. Cao, Z. Liu, P. Verwilst, S. Koo, P. Jangjili, J. S. Kim and W. Lin, *Chem. Rev.*, 2019, **119**, 10403–10519.
6 D. Ray and P. K. Bharadwaj, *Inorg. Chem.*, 2018, **47**, 2252–2254.
7 H. Sung Jung, J. Hye Han, Y. Habata, C. Kang and J. Seung Kim, *Chem. Commun.*, 2011, **47**, 5142–5144.
8 U. Reddy, H. Agarwalla, N. Taye, S. Ghorai, S. Chattopadhyay and A. Das, *Chem. Commun.*, 2014, **50**, 9899–9902.
9 Q. Ma, X. Fang, J. Zhang, L. Zhu, X. Rao, Q. Lu, Z. Sun, H. Yu and Q. Zhang, *J. Mater. Chem. B*, 2020, **8**, 4039–4045.
10 D. Chao and Y. Zhang, *Sens. Actuators, B*, 2017, **245**, 146–155.
11 E. Faggi, R. Gavara, M. Bolte, L. Fajarí, L. Juliá, L. Rodríguez and I. Alfonso, *Dalton Trans.*, 2015, **44**, 12700–12710.
12 E. Garribba and G. Micera, *J. Chem. Educ.*, 2006, **83**, 1229–1232.
13 X. F. Yang, Q. Huang, Y. Zhong, Z. Li, H. Li, M. Lowry, J. O. Escobedo and R. M. Strongin, *Chem. Sci.*, 2014, **5**, 2177–2183.
14 R. R. Nair, S. Debnath, S. Das, P. Wakchaure, B. Ganguly and P. B. Chatterjee, *ACS Appl. Bio Mater.*, 2019, **2**, 2374–2387.
15 E. Bald, E. Kaniowska, G. Chwatko and R. Glowacki, *Talanta*, 2000, **50**, 1233–1243.

European Journal of Medicinal Chemistry 238 (2022) 114465

Contents lists available at ScienceDirect

European Journal of Medicinal Chemistry

journal homepage: www.elsevier.com/locate/ejmech

Design, synthesis of DNA-interactive 4-thiazolidinone-based indolo-/pyrroloazepinone conjugates as potential cytotoxic and topoisomerase I inhibitors

Manasa Kadagathur [a], Sandip Patra [a], Geetanjali Devabattula [b], Joel George [c], Regur Phanindranath [c], Arbaz Sujat Shaikh [a], Dilep Kumar Sigalapalli [a], Chandraiah Godugu [b,*], Narayana Nagesh [c,*], Neelima D. Tangellamudi [a,*], Nagula Shankaraiah [a,*]

[a] Department of Medicinal Chemistry, National Institute of Pharmaceutical Education and Research (NIPER), Hyderabad, 500037, India
[b] Department of Regulatory Toxicology, National Institute of Pharmaceutical Education and Research (NIPER), Hyderabad, 500037, India
[c] CSIR-Centre for Cellular and Molecular Biology, Medical Biotechnology Complex, ANNEXE II, Uppal Road, Hyderabad, 500007, India

ARTICLE INFO

Keywords:
Indoloazepinone
Pyrroloazepinone
Thiazolidinone
Anticancer
DNA intercalation
Topoisomerase I inhibition
Molecular modeling

ABSTRACT

With the rising cancer incidence and mortality globally, there is a prerequisite for effective design strategies towards the discovery of newer small molecular entities in chemotherapy. Hence, a series of new thiazolidinone-based indolo-/pyrroloazepinone conjugates was designed, synthesized *via* molecular hybridization, and evaluated for their *in vitro* cytotoxicity potential and DNA topoisomerase I and II inhibition. Among this series, conjugate **11g** emerged as the most active compound with an IC_{50} value of 1.24 μM against A549 and 3.02–10.91 μM in the other tested cancer cell lines. Gratifyingly, **11g** displayed 43-fold higher selectivity towards A549 cancer cells as compared to the non-cancer cells. Subsequently, conjugate **12g** also demonstrated significant cytotoxicity against SK-MEL-28 cells. Basing the *in vitro* cytotoxicity results, SAR was established. Later, the conjugates **11g** and **12g** were further evaluated for their apoptosis-inducing ability, which was quantified by flow cytometric analysis, DNA-binding, Topo I inhibitory activity and IC_{50} value calculation. Molecular modeling studies provided profound insights about the binding nature of these compounds with DNA-Topo I complex. *In silico* ADME/T and prediction studies corroborated the drug-likeness of the two investigated compounds. TOPKAT toxicity profiling studies demonstrated the compounds' safety in many animal models with a minimal toxicological profile. Encouraging results obtained from *in vitro* and *in silico* studies could put this series of conjugates at the forefront of cancer drug discovery.

1. Introduction

Cancer is a multifaceted global health concern cutting through society and demanding the development of novel therapeutics to stop its progression. A great number of chemotherapeutic agents has been discovered till date, however, most of them encounter the setback of serious adverse effects, safety concerns and most importantly multidrug resistance [1–7]. Small molecules targeted compounds have become mainstream cancer treatment modalities given their improved safety and efficacy. DNA remains to be an interesting and a rewarding target in cancer chemotherapy [8]. Cytotoxic DNA-binding agents interact with DNA either *via* intercalation, groove binding or by alkylating the base pairs [9–12]. Topoisomerases, known as the '*cellular magicians*', are ubiquitous enzymes that play a pivotal role in important cellular processes such as DNA replication, transcription, recombination, repair, and chromatin remodeling. Topoisomerase I (Topo I) inhibitors act via stabilization of the transient topoisomerase I–DNA complex ultimately resulting in cell death. Due to this important role played by Topo I in cellular functions, it is an important target for the anticancer drug discovery [13].

Nitrogen-containing heteroaryl-fused azepinone class of molecules such as indoloazepinones and pyrroloazepinones (Fig. 1) demonstrates remarkable medicinal properties; one of them being, antitumor activity. Natural and synthetic compounds containing these *privileged scaffolds*

* Corresponding authors.
E-mail addresses: chandra.niperhyd@gov.in (C. Godugu), nagesh@ccmb.res.in (N. Nagesh), tdneelima@gmail.com (N.D. Tangellamudi), shankar@niperhyd.ac.in (N. Shankaraiah).

https://doi.org/10.1016/j.ejmech.2022.114465
Received 18 February 2022; Received in revised form 25 April 2022; Accepted 12 May 2022
Available online 18 May 2022

exhibited extremely encouraging inhibition of a panel of enzymes such as cyclin-dependent kinases (CDKs) [14–16], checkpoint kinases (Chks) [17], mitochondrial malate dehydrogenase (mMDH) [18], glycogen synthase kinase-3β (GSK-3β) [17,19], protein tyrosine phosphatase 1B (PTP1B) [20], and mitogen-activated protein kinase-1 (MAPK-1) [21]. Additionally, inhibition of tubulin polymerization [22] and topoisomerase I [10] are the recently explored potentials of this class of antitumor agents. Most recently, rucaparib, a fused-azepinone-based drug, has been approved by the FDA as a third-line treatment of mutated *BRCA*-comprising ovarian cancer [23].

Next, thiazolidinone is also a biologically important five-membered heterocyclic moiety having a wide-ranging biological activity. 4-Thiazolidinones demonstrated their antiproliferative potential by acting on various molecular targets including JNK stimulating phosphatase-1 (JSP-1) [24], tumor necrosis factor-α (TNF-α) [25], integrin α/β receptor [26], histone deacetylase [27], SHP-2 [28], BH3 domain and Bcl-XL [29], microtubules/tubulin assembly [30–38], to name a few. Lately, 4-thiazolidinone derivatives were also reported for their diverse biological applications such as peroxisome proliferator-activated receptor γ-binders [39,40], follicle-stimulating hormone agonists [41,42], cystic fibrosis transmembrane conductance regulator inhibitors [43,44] and antioxidants [45–47].

Although, a huge number of anticancer agents having indole and pyrrole as the pharmacophores has been established and reported, their target selectivity has been a foremost challenge till date. There is an extremely high scope for exploration of the pharmacological significance of heteroaryl-fused azepinones, especially towards the development of potent anticancer agents. Particularly, the nifty extensions of numerous functional groups on azepinoindolones would encounter derivatization yielding hybrids or drug substances possessing varying mechanisms of action and possibly with good pharmacological values. In this connection, herein we report a new series of 4-thiazolidinone-based indolo-/pyrroloazepinone conjugates (Fig. 1) and investigated their antitumor activity on human cancer cell lines and topoisomerase I in a cell-free system along with DNA binding studies. This research was mainly aimed to search and develop more potent DNA topoisomerase I inhibitors by mimicking the pharmacological significance of two pharmacophores, such as thiazolidinones and heteroaryl-fused azepinones in a single entity, *via* molecular hybridization strategy.

2. Results and discussion

2.1. Chemistry

In continuation of our research efforts towards the development of new and efficient anti-proliferative agents [48–50], herein, a library of thiazolidinone-based indolo-/pyrroloazepinone conjugates was designed and synthesized. Initially, indoloazepinone and pyrroloazepinone key starting materials **3**–**4** were obtained according to their previous reports [10,51]. Further, *N*-methylation was performed by treating **3** and **4** with methyl iodide in the presence of K_2CO_3 and acetonitrile as solvent to provide the key intermediates **5** and **6**, respectively, as depicted in Scheme 1.

Concurrently, substituted and unsubstituted benzyl/phenethyl thiazolidinones **10** were prepared upon reacting the corresponding benzyl/phenethylamines **7** with chloroacetyl chloride **8** in DMF to yield the respective amides **9**. Then, **9** undergoes cyclization in the presence of ammonium thiocyanate to give the desired thiazolidinones **10** in good to excellent yields (Scheme 2).

Next, the attempts were made to obtain the desired compound **11a**

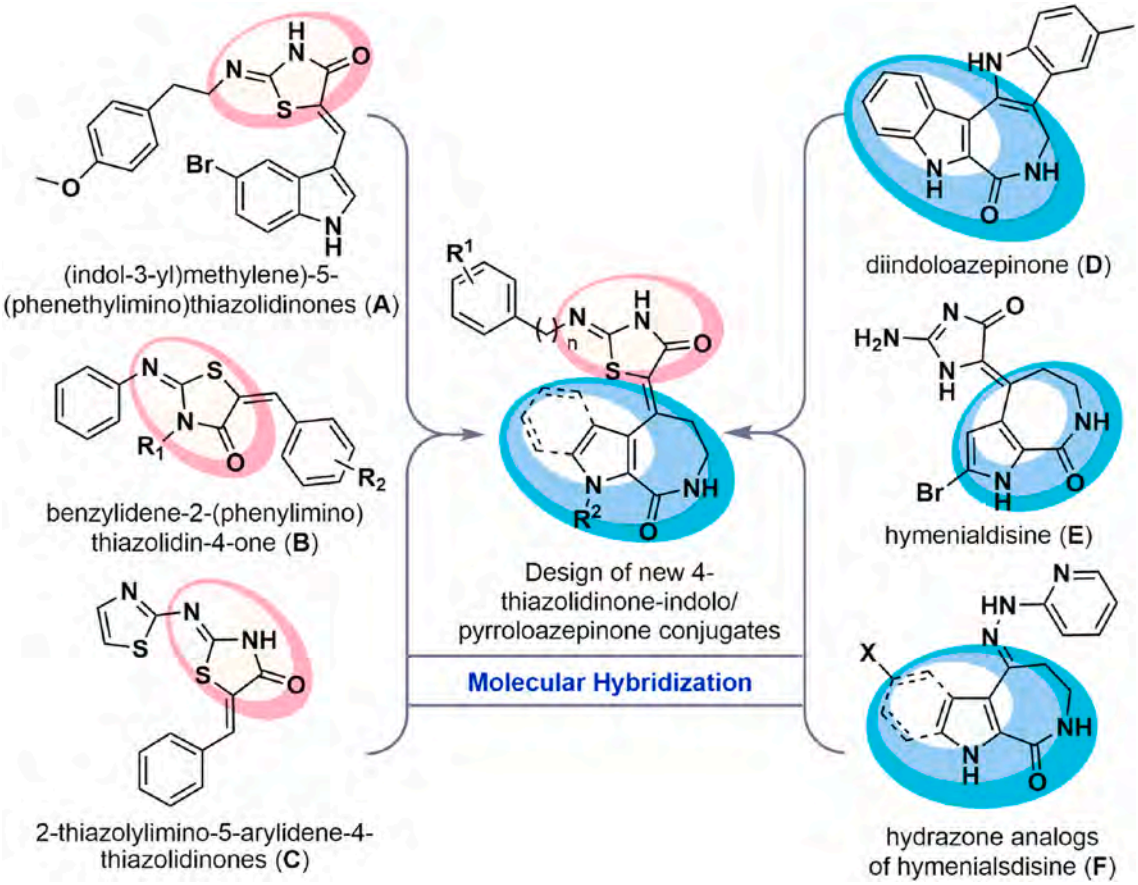

Fig. 1. Representative examples of bioactive thiazolidinones and indolo-/pyrroloazepinones and rationale of designing their new conjugates by molecular hybridization approach.

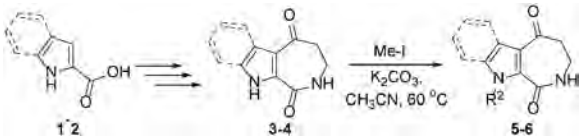

Scheme 1. Synthetic route for substituted indoloazepinones and pyrroloazepinones.

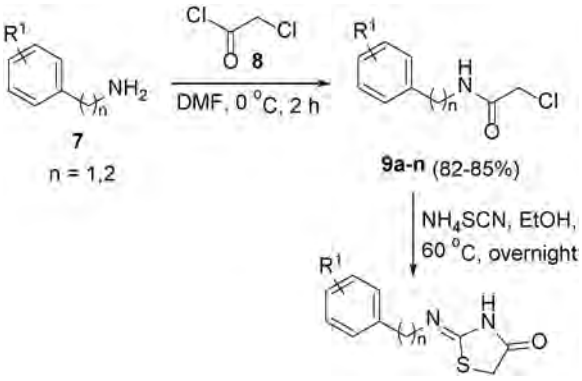

Scheme 2. Synthesis of substituted 2-iminothiazolidin-4-ones **10a-n**.

by optimizing the reaction conditions for conjugation between indoloazepinone **5a** and 2-(arylimino)thiazol-4-one **10a**, as presented in Table 1.

Finally, the substituted and unsubstituted indolo-/pyrrolozepinones (**3**–**6**) and 2-imino-4-thiazolidinones (**10a-n**) were reacted to obtain the corresponding products **11a-l** and **12a-m** in good to excellent yields (Table 2).

2.2. Biological evaluation

2.2.1. Cytotoxicity assays

The synthesized conjugates were screened for their *in vitro* cytotoxicity against a panel of human cancer cell lines (A549, HCT-116, SK-MEL-28, HT-29 and MCF-7) along with normal cell line (NRK) and were compared with the drug standards 5-fluorouracil (5-FU) and doxorubicin by performing MTT (3-(4,5-dimethylthiazol-2-yl)-2,5-diphenyltetrazolium bromide) staining assay. The IC_{50} values (concentration necessary to inhibit 50% of growth in cancer cells) obtained are listed in Table 3. Compound **11g** was identified as the most potent indoloazepinone-thiazolidinone conjugate with an IC_{50} value of 1.24 ± 0.53 μM in the A549 cell line.

Likewise, it displayed significant cytotoxicity (IC_{50} values ranging between 3.02 ± 0.70 and 10.91 ± 0.01 μM) in all the other tested cancer cell lines. It is interesting to observe that **11g** exhibited a 43-fold selectivity towards the cancer cell line (A549) as compared to NRK, thus revealing its excellent safety profile against normal cells. Remarkably, **11d**, **11h** and **11k** also displayed notable cytotoxicity against A549, SK-MEL-28 and MCF-7 cell lines with IC_{50} values < 10 μM. Amongst the pyrroloazepinone-thiazolidinone conjugates, **12g** displayed significant apoptosis in all the tested cancer cell lines (IC_{50} values ranging from 4.15 ± 0.05 to 9.08 ± 0.3 μM), 0.05 to 9.08 ± 0.3 μM), with the highest activity being seen in SK-MEL-28 cell line (IC_{50} value of 4.15 ± 0.05 μM). The 50% inhibition by **12g** was 10-fold less in non-cancerous cells than in SK-MEL-28. Other pyrroloazepinone-based analogues such as **12b**, **12j** and **12m** also exhibited significant range of IC_{50} values between 8.14 and 4.25 μM in various cancer cell lines. The structure-activity relationship (SAR) of the entitled compounds was furnished based on the *in vitro* cytotoxicity results and is illustrated in Fig. 2.

Further detailed studies to explore the mechanism involved in the cell growth inhibition, various assays including apoptotic studies, DNA binding studies and Topo I inhibition were performed on the most active compounds, one each from indolo- and pyrroloazepinone series of conjugates **11g** and **12g**.

2.2.2. Apoptosis induction studies

One lead molecule each from both indoloazepinone (**11g**) and pyrroloazepinone (**12g**) conjugates were chosen and their apoptosis-inducing capabilities were investigated by performing various assays such as AO/EB, DAPI, DCFDA and clonogenic growth inhibition and the results are detailed.

2.2.2.1. Morphological observations. The effect of **11g** and **12g** on the cellular morphology was examined by treating A549 and SK-MEL-28 cells, respectively, with the compounds under investigation at different concentrations. After incubating the cancer cells with **11g** and **12g** for about 48 h, changes in their morphology were observed under a phase-contrast microscope and compared with a drug standard – camptothecin (CPT). Various characteristic apoptotic features [52], such as cell shrinkage, cell membrane disruption and a decrease in the number of viable cells can be observed in the captured images of the treated cells (Fig. 3). From the results, it is evident that there is a dose-dependent

Table 1
Optimization of the reaction conditions for the synthesis of indoloazepinone-thiazolodinone conjugate **11a**[a].

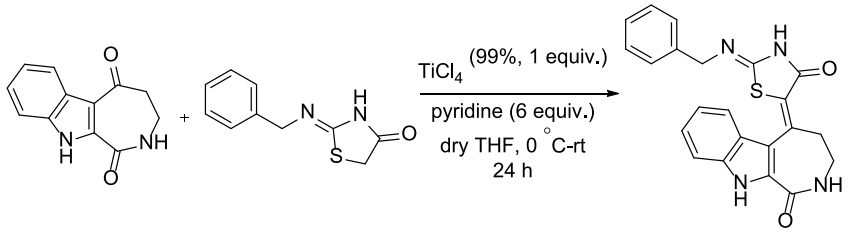

Entry	Reagent (X equiv.)	Solvent	Temp.	Time (h)	Yield (%)[b]
1	$TiCl_4$ (1 M, 2), pyridine (3.5)	CH_2Cl_2	0 °C-rt	12	–
2	$Ti(O^iPr)_4$ (2), pyridine (3.5)	THF	0 °C-rt	20	–
3	NaHMDS (0.9)	THF	−20 °C	24	–
4	$TiCl_4$ (99%, 4), pyridine (4.5)	THF	0 °C-rt	24	40
5	$TiCl_4$ (99%, 2), pyridine (5)	THF	0 °C-rt	24	73
6	$TiCl_4$ (99%, 1), pyridine (6)	THF	0 °C-rt	24	82

[a] Reagents and conditions: All the reactions were carried out under N_2 atmosphere, **5a** (1 mmol), **10a** (1.5 equiv.) in dry solvent (10 mL).
[b] Isolated yields.

Table 2
Synthesis of 2-iminothiazolidin-4-one conjugates of indoloazepinone **11a-l** and pyrroloazepinone **12a-m**[a] along with their respective % yields.[b]

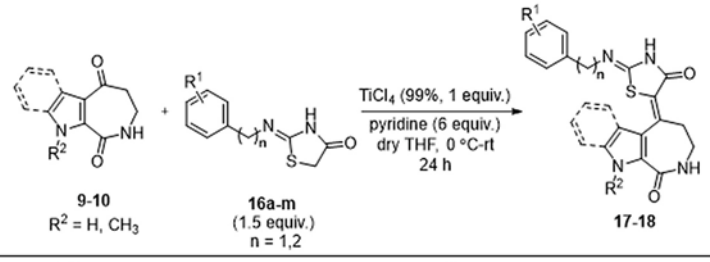

9-10
R^2 = H, CH_3

16a-m
(1.5 equiv.)
n = 1,2

17-18

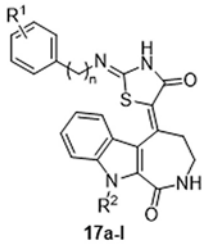

17a-l

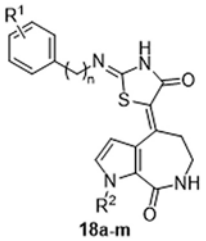

18a-m

17a: n = 1; R^1 = R^2 = H (82%)
17b: n = 1; R^1 = 3-Cl; R^2 = H (81%)
17c: n = 1; R^1 = 4-F; R^2 = H (76%)
17d: n = 1; R^1 = 4-OCH_3; R^2 = H (92%)
17e: n = 1; R^1 = 3,4-diOCH_3; R^2 = H (95%)
17f: n = 1; R^1 = 4-Cl; R^2 = H (79%)
17g: n = 1; R^1 = 4-CH_3; R^2 = H (91%)
17h: n = 1; R^1 = 4-$C(CH_3)_3$; R^2 = H (92%)
17i: n = 1; R^1 = -(1,3-dioxole); R^2 = H (87%)
17j: n = 1; R^1 = H; R^2 = CH_3 (94%)
17k: n = 2; R^1 = 4-OCH_3; R^2 = H (92%)
17l: n = 2; R^1 = 4-F; R^2 = H (87%)

18a: n = 1; R^1 = R^2 = H (84%)
18b: n = 1; R^1 = 4-OCH_3; R^2 = H (97%)
18c: n = 1; R^1 = 4-CF_3; R^2 = H (86%)
18d: n = 1; R^1 = 4-Cl; R^2 = H (86%)
18e: n = 1; R^1 = 3-Cl; R^2 = H (81%)
18f: n = 1; R^1 = 2-Cl; R^2 = H (87%)
18g: n = 1; R^1 = 4-CH_3; R^2 = H (92%)
18h: n = 1; R^1 = 4-$C(CH_3)_3$; R^2 = H (93%)
18i: n = 1; R^1 = 4-F; R^2 = H (80%)
18j: n = 1; R^1 = -(1,3-dioxole); R^2 = H (86%)
18k: n = 1; R^1 = 4-OCH_3; R^2 = CH_3 (90%)
18l: n = 2; R^1 = R^2 = H (85%)
18m: n = 2; R^1 = 4-OCH_3; R^2 = H (89%)

[a] Reagents and conditions: **3**–**6** (1 mmol), **10a-n** (1.5 equiv.), $TiCl_4$ (99%, 1 equiv.), dry pyridine (6 equiv.), dry THF (10 mL), 0 °C-rt, N_2, 24 h.
[b] Isolated yields.

effect of both the compounds, **11g** and **12g**, on the viability of the treated-A549 and treated-SK-MEL-28 cells, respectively, in comparison to the corresponding untreated ones.

2.2.2.2. DAPI nucleic acid staining. DAPI (4′-6-diamidino-2-phenylindole) is a fluorescent dye, mainly employed to stain the nucleus of the live cells with intact membrane light blue, while the apoptotic cells impart a bright blue fluorescence due to chromatin condensation [53]. To investigate the nuclear morphological changes in A549 and SK-MEL-28 cells, DAPI staining was performed after a 48 h treatment with compounds **11g** and **12g**, respectively, and the images were captured by a fluorescence microscope and compared with camptothecin, as given in Fig. 4. In this investigation, it was observed that, while the control cells showed intact cell membrane and nucleus with normal morphology, those treated with compounds **11g** and **12g**, akin to camptothecin-treated cells, displayed typical apoptotic nuclear morphological changes, such as horseshoe shaped, pyknotic/fragmented bright nuclei and chromatin condensation.

2.2.2.3. Acridine orange/ethidium bromide (AO/EB) staining. AO/EB staining is a dual staining technique used to accurately distinguish live, apoptotic and necrotic cells. Herein, AO pervades cells with intact cellular membranes (normal and early apoptotic cells), thus imparting a green fluorescence, whereas EB penetrates only those cells with damaged membranes (including late apoptotic and dead cells) and stains them orange-red [54]. From Fig. 5, it can be construed that the control cells maintained normal morphology and as a result appeared green in color. On the other hand, the **11g** and **12g** treated cells showed green fluorescence along with morphological hallmarks of apoptosis such as cell shrinkage, fragmentation into apoptotic bodies, membrane bleb formation and condensation of chromatin. Additionally, the late apoptotic cells displayed condensed chromatin with their nuclei stained red by EB similar to the camptothecin-treated cells. These results imply that, both compounds **11g** and **12g** induced apoptosis in A549 and SK-MEL-28 cells, respectively, in a concentration-dependent manner.

2.2.2.4. ROS generation (DCFDA staining). ROS (reactive oxidative species) are highly reactive, short-lived species that perform a vital role in the immune system and regulation of normal physiological functioning of a cell. ROS, when present in excess, prove to be deleterious and trigger oxidative stress, thereby, induce apoptosis by damaging proteins, cell membranes, lipids, nucleic acids and organelles. Having said that, most of the cytotoxic agents tend to generate ROS as a mechanism to induce apoptosis. DCFDA (2′,7′-dichlorofluorescein diacetate) fluorescence assay has been employed to analyze the ROS generation [55] in the lung cancer (A549) and human melanoma (SK-MEL-28) cells upon treatment with investigating compounds **11g** and **12g**, respectively, at various concentrations and the images were captured with fluorescence microscope (Fig. 6). ROS generation was observed even in the camptothecin-treated A549 and SK-MEL-28 cells as a result of apoptosis induction. From the images, it can be construed that both the compounds induce ROS generation and an increase in the green fluorescence is observed dose-dependently in comparison to the control cells.

2.2.2.5. In vitro cell migration (wound healing) assay. Tumor metastasis,

Table 3
In vitro cytotoxicity (IC_{50} values in μM) data for the synthesized heteroarylazepinone-4-thiazolidinone conjugates **11a-l** and **12a-m**.

Compound	[a]A549	[b]HCT-116	[c]SK-MEL-28	[d]HT-29	[e]MCF-7	[f]NRK
11a	48.18 ± 4.83	34.38 ± 1.9	29.84 ± 1.67	31.82 ± 4.07	31.02 ± 3.86	–
11b	33.74 ± 2.41	25.22 ± 0.47	23.77 ± 1.52	>50	28.09 ± 2.4	–
11c	36.50 ± 3.60	30.84 ± 2.31	>50	38.03 ± 2.69	40.29 ± 5.01	–
11d	3.73 ± 0.78	17.54 ± 0.57	9.68 ± 0.15	12.35 ± 0.12	6.33 ± 0.261	–
11e	29.99 ± 1.89	16.36 ± 0.18	25.07 ± 3.7	>50	23.66 ± 2.46	–
11f	33.64 ± 0.42	22.68 ± 2.12	>50	39.91 ± 3.40	46.77 ± 1.65	–
11g	1.24 ± 0.53	6.55 ± 1.04	3.02 ± 0.70	10.91 ± 0.01	8.03 ± 0.09	53.18 ± 0.1
11h	19.34 ± 1.54	15.87 ± 1.56	8.97 ± 1.35	13.63 ± 0.17	9.01 ± 0.05	–
11i	>50	21.35 ± 1.18	>50	36.46 ± 2.31	31.39 ± 0.79	–
11j	>50	>50	>50	>50	>50	–
11k	20.47 ± 0.84	18.63 ± 0.32	3.49 ± 0.57	15.03 ± 0.59	9.41 ± 0.25	–
11l	>50	>50	>50	>50	>50	–
12a	26.88 ± 1.15	49.7 ± 4.45	38.36 ± 2.13	36.52 ± 1.2	31.07 ± 1.77	–
12b	18.34 ± 0.14	19.35 ± 1.74	12.06 ± 0.28	11.53 ± 1.77	6.24 ± 0.36	–
12c	>100	>100	>100	>50	>100	–
12d	>100	>100	>100	>100	>100	–
12e	35.2 ± 4.45		34.65 ± 2.54	35.27 ± 2.51	20.66 ± 2.67	–
12f	>100	>50	>100	>100	21.18 ± 2.38	–
12g	9.08 ± 0.3	4.76 ± 2.41	4.15 ± 0.05	6.83 ± 0.77	8.15 ± 0.52	41.92 ± 1.16
12h	43.87 ± 7.49	>100	23.47 ± 2.01	43.38 ± 3.53	18.91 ± 0.61	–
12i	22.39 ± 1.79	16.90 ± 2.57	11.16 ± 1.03	25.98 ± 4.84	43.10 ± 1.43	–
12j	19.86 ± 0.46	4.25 ± 0.37	11.16 ± 1.03	16.46 ± 0.82	4.31 ± 0.33	–
12k	>100	>100	>100	32.38 ± 3.94	>100	–
12l	19.47 ± 1.25	17.83 ± 2.84	12.35 ± 2.72	24.86 ± 4.85	20.96 ± 0.45	–
12m	15.96 ± 0.26	10.8 ± 0.43	7.86 ± 0.32	8.14 ± 0.31	6.47 ± 0.38	–
5-FU	11.42 ± 0.43	9.88 ± 2.94	14.64 ± 1.69	23.9 ± 3.7	21.11 ± 3.76	
dox	10.28 ± 0.92	7.41 ± 1.12	1.64 ± 0.17	–	5.17 ± 0.91	–
camptothecin	0.47 ± 0.02	–	2.26 ± 0.11	–	–	–

[a]Non-linear regression analysis of 50% inhibitory concentration determined by taking the mean value of n = 3 independent MTT assay experiments; treatment time: 48 h.
[a] A549 - lung cancer cells.
[b] HCT-116 - human colorectal carcinoma.
[c] SK-MEL-28 - human melanoma cell line.
[d] HT-29 – caucasian colon adenocarcinoma.
[e] MCF-7 - breast adenocarcinoma.
[f] NRK – normal rat kidney epithelial cells; 5-FU - 5-fluorouracil, dox – doxorubicin.

the process of movement of malignant cancer cells from a primary site to distant sites/organs, is one of the major causes of death in cancer patients. The effect of both, indoloazepinone (**11g**) and pyrroloazepinone (**12g**) conjugates on the collective cell migration in A549 and SK-MEL-28 cell lines, respectively, can be studied by performing a wound healing assay [56]. In this investigation, an artificial wound (scratch) is introduced in the respective **11g**- and **12g**-treated and untreated cells using a sterile pipette tip (200 μL) and the images were captured at 0 and 48 h for comparison. The results given in Fig. 7 infer that, while the wound in control was healed, there was inhibition in the cell migration observed in the case of both **11g**- and **12g**-treated cells after 48 h of treatment, in a concentration-dependent manner.

2.2.2.6. Cell growth inhibition assay. Clonogenic or the cell growth inhibition assay measures the colony-forming ability of the cancer cells which helps in determining the capability of the highly proliferative cancer cells to develop into solid tumors [57]. This assay was performed on A549 and SK-MEL-28 cells treated with the most active compounds **11g** and **12g**, respectively, at different concentrations in comparison with the control (untreated cells) (Fig. 8). Upon observation of the colonies formed after seven days of treatment, apparent reduction in their number was observed dose-dependently, thus, indicating the potency of the lead compound **11g** and **12g** in inhibiting the colony-forming potential of the A549 and SK-MEL-28 cells, respectively.

2.2.2.7. Annexin V-FITC/PI staining assay. To quantify the apoptosis induced by investigated compounds **11g** and **12g**, flow cytometric analysis was performed by using Annexin V-FITC/PI staining assay. Annexin V binds to the negatively charged phosphatidylserine (PS), a hallmark of apoptosis, exposed on the outer cellular membrane thus imparting fluorescence. Propidium iodide (PI) is excluded by the living cells with intact plasma membrane. Therefore, cells which stained positive for annexin V-FITC/PI represent those in the late apoptotic stage that have lost membrane integrity [57]. This assay offers a method to detect cells in different stages, such as, necrotic cells (Q1-UL; AV-/PI+), live cells (Q2-LL; AV-/PI-), early apoptotic cells (Q3-LR; AV+/PI-), and late apoptotic cells (Q4-UR; AV+/PI+). Upon treatment with various concentrations of compound **11g**, A549 cells demonstrated increased AV/PI binding in comparison to control cells (Fig. 9). (2.97%) An increase in the necrotic cell population (from 4.8% at 0.625 μM to 5.96% at 2.5 μM) was observed in a dose dependent manner. An increase in the late apoptotic cells was also seen with an increasing concentration of **11g** from 0.625 μM to 1.25 μM. However, with further increase in the dose of the investigated compound resulted in a decrease in the late apoptotic cell population (3.09%) and rise in the necrotic cells. Similar inference was construed upon quantification of apoptosis induction by compound **12g** in SK-MEL-28 cell line, wherein a dose-dependent increase in the necrotic cell population (from 4.84% at 2.08 μM to 7.38% at 8.3 μM) was observed in comparison with the control cells (3.85%). Also, an increase in the population of late apoptotic cells was observed till 4.16 μM and further increase in the concentration decreased their population with appearance of higher necrotic cells. Results of both the compounds have been compared with a drug standard, camptothecin as shown in Fig. 9.

2.2.3. DNA binding studies

DNA is an important biomolecule in all the living systems. Most of biological assays mentioned above involve the interaction of compounds directly or indirectly with ds DNA. The study on the interaction of compounds with DNA will throw enough light on the extent and nature of compound's interaction with ds DNA (B-DNA). Building on our previous research [10], and as an addition to the assessment of biological activities of the two active compounds **11g** and **12g**, spectroscopic studies were performed with an aim to understand their nature of interaction with DNA.

2.2.3.1. UV–visible studies. Absorption spectroscopy is one of the most widely used techniques to study the intermolecular interactions between small molecules and the DNA. The interaction of DNA with its ligand may alter the absorption maximum (λ_{max}) of the former depending on the type of intermolecular interaction. Hypochromic shift is known as the characteristic feature of the molecules showing DNA-interaction. It

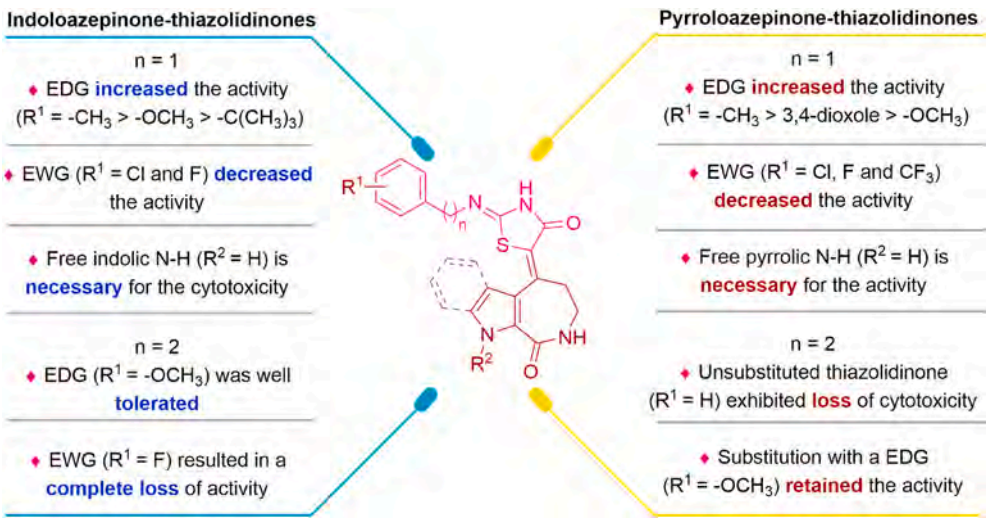

Fig. 2. The structure-activity relationship (SAR) of indoloazepinone and pyrroloazepinone conjugates of 4-thiazolidinones.

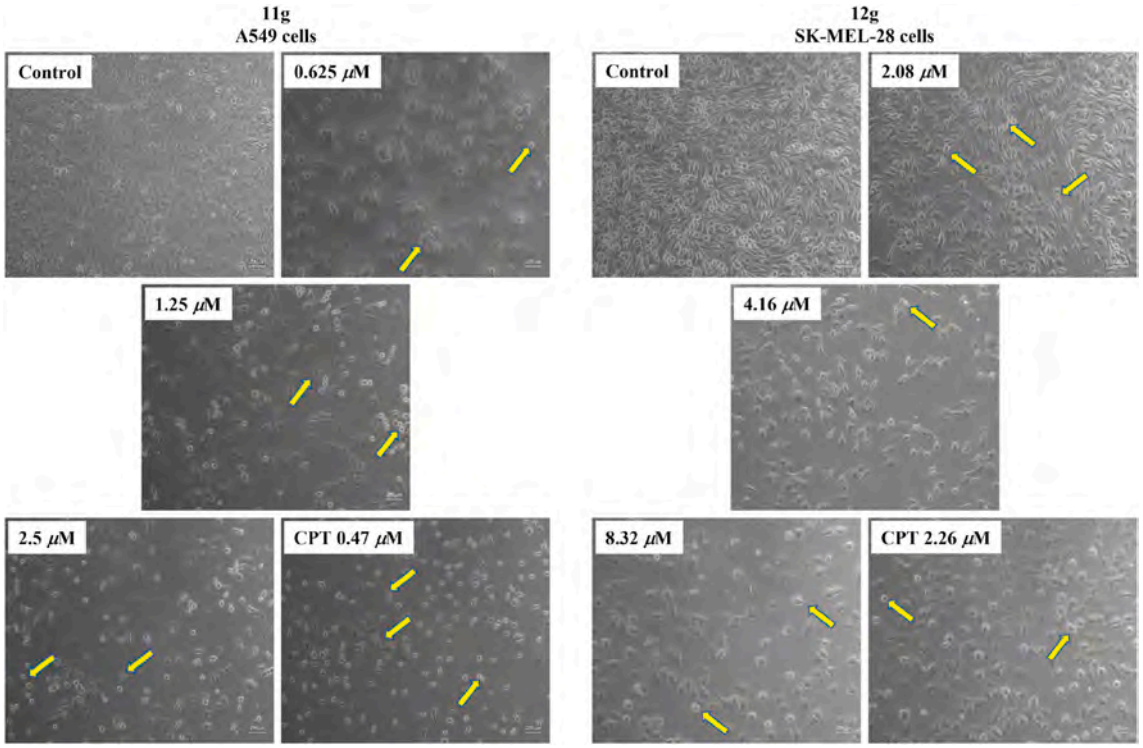

Fig. 3. Morphological changes observed after treatment with **11g** (at concentrations of 0.625, 1.25 and 2.5 μM in A549 cell line) and **12g** (at concentrations of 2.08, 4.16 and 8.32 μM in SK-MEL-28 cell line) for 48 h and compared with control/untreated cells and camptothecin (CPT)-treated cells. All the images were captured using a phase contrast microscope at 100X magnification.

has been reported that the extent of hypochromic shift indicates the strength of the intercalative binding [58]. In the present study, λ_{max} of the ligand **11g** at 370 nm gradually reduced on the addition of CT-DNA, albeit without any alterations in the absorption wavelength (Fig. 10A). It is worth noting that hypochromicity occurring after the addition of the ligand is ascribed to the interaction between the electronic states of the ligands and those of the DNA bases [59]. Upon continuous addition of CT-DNA to the ligand solution (**11g**), a dose-dependent hypochromicity was observed in the absorption band of ligand at 370 nm (Fig. 10A) revealing the intimate association of the compound with the CT-DNA *via* intercalation. On the other hand, treatment of compound **12g** with the CT-DNA resulted in hypochromicity of the absorption band (at **12g**, λ maxima at around 355 nm) without bathochromic shift (Fig. 10B). In both the titrations, an isobestic point is observed at 278 nm and at 300 nm, with **11g** and **12g** compounds respectively, where the complex of compound and the DNA act as a single component and give the same absorbance.

2.2.3.2. Circular dichroism spectroscopy. The conformational changes occurring in the nucleic acid structure or changes in the environmental conditions following its interaction with the molecule can potentially be studied by circular dichroism (CD). The CD spectrum of the CT-DNA presented a positive band at 275 nm and a negative band at 245 nm owing to π–π base stacking and right-hand helicity, respectively.

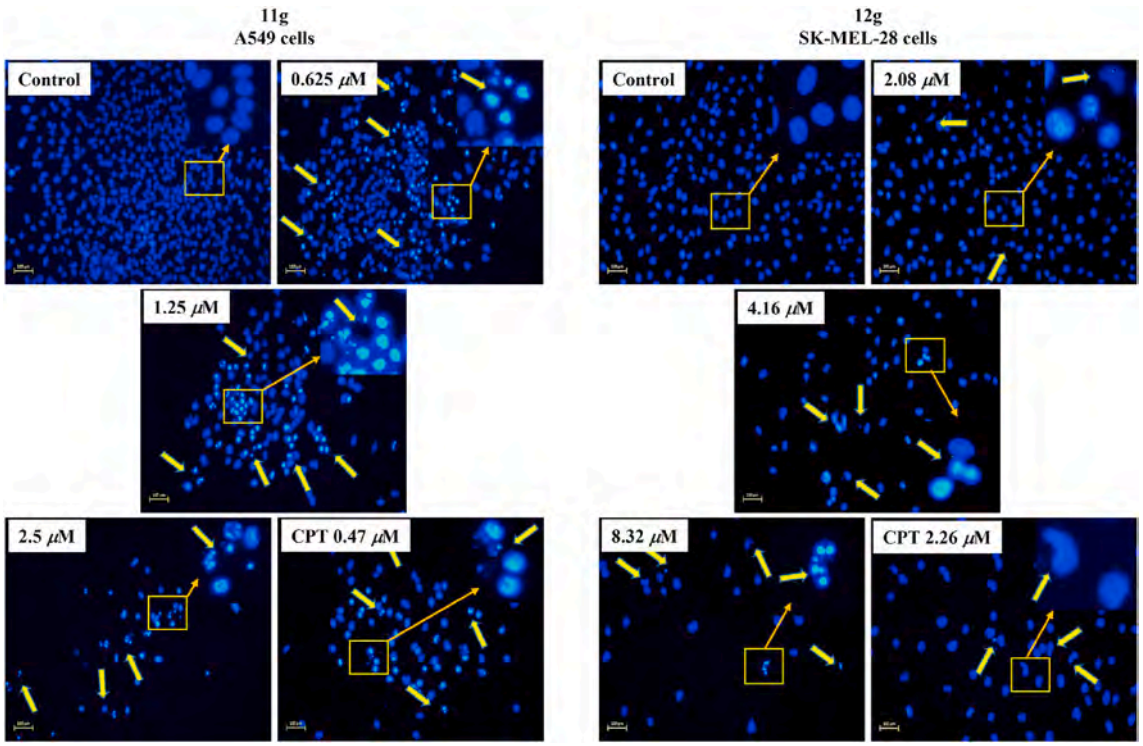

Fig. 4. DAPI staining images displaying the nuclear morphology of A549 cells treated with camptothecin and compounds **11g** (0, 0.625, 1.25 and 2.5 μM) and **12g** (2.08, 4.16 and 8.32 μM) for 48 h in comparison with control and camptothecin-treated cells. The images were captured with a fluorescence microscope at a magnification of 200X.

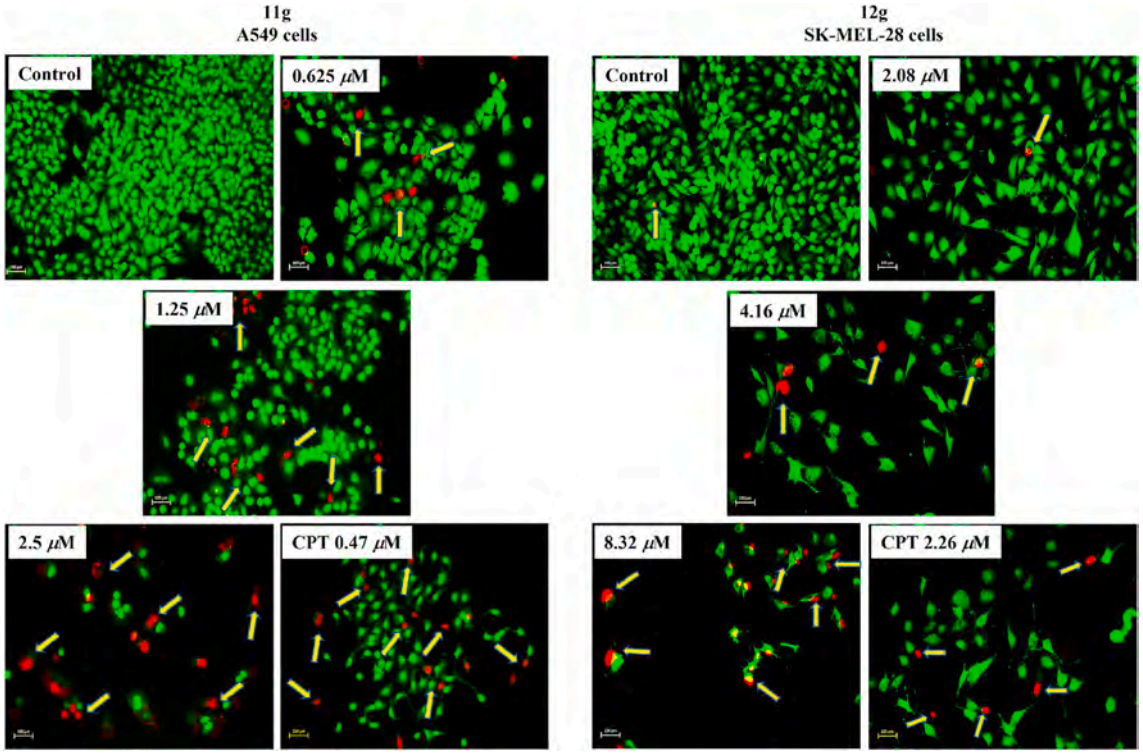

Fig. 5. AO/EB staining of A549 and SK-MEL-28 cells treated with and without compound **11g** and **12g**, respectively, in comparison with camptothecin (CPT) after 48 h. Images were captured at 200X magnification under a fluorescence microscope.

When **11g** was added at a concentration of 10 μM to the same concentration of CT-DNA solution (DNA:**11g**, 1:1), hypochromicity was observed in the positive band at 275 nm, indicating the melting of the DNA-compound complex (Fig. 11A). On further increasing the concentration of compound **11g** (DNA:**11g**, 1:2), the positive band at 275 nm exhibited further decrease in its intensity, which is an indication of the

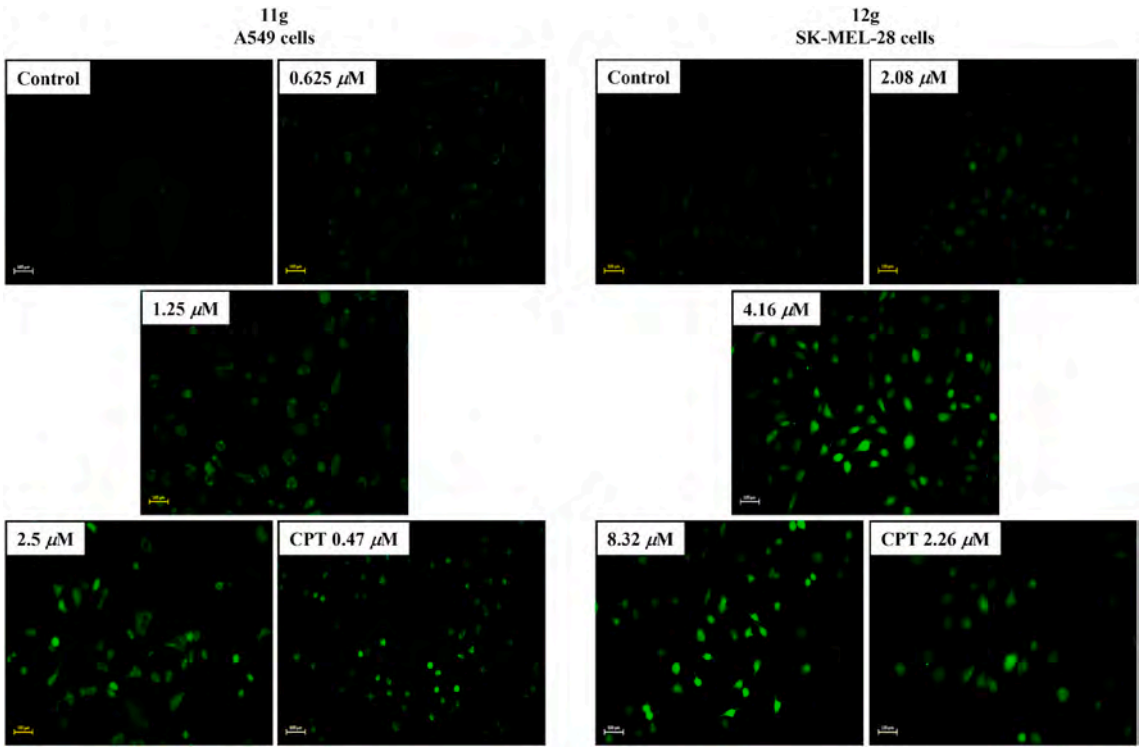

Fig. 6. DCFDA staining in A549 and SK-MEL-28 cancer cells after treatment with various concentrations of compounds **11g** and **12g** for 48 h and compared with control with camptothecin-treated cells as reference. Images were captured at 200X magnification under a fluorescence microscope.

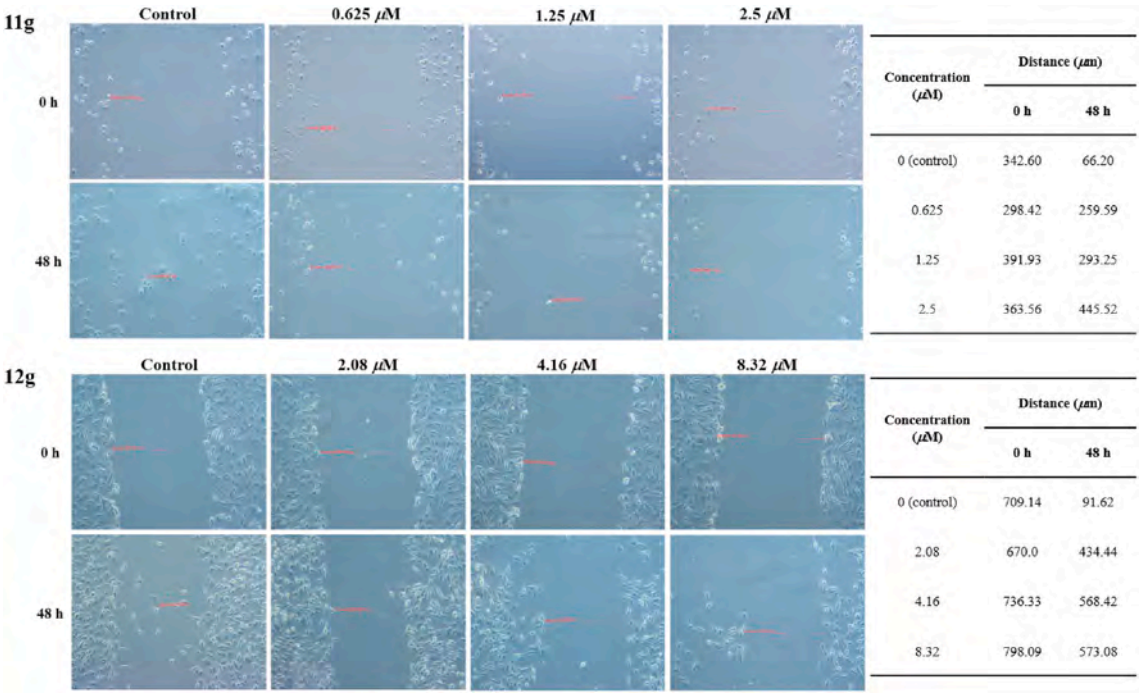

Concentration (μM)	Distance (μm)	
	0 h	48 h
0 (control)	342.60	66.20
0.625	298.42	259.59
1.25	391.93	293.25
2.5	363.56	445.52

Concentration (μM)	Distance (μm)	
	0 h	48 h
0 (control)	709.14	91.62
2.08	670.0	434.44
4.16	736.33	568.42
8.32	798.09	573.08

Fig. 7. Effect of compounds **11g** and **12g** on the migration potential of A549 and SK-MEL-28 cancer cell lines, respectively, at corresponding concentrations. Scratch/wound was introduced using a sterile pipette tip and compared with controlled (DMSO-treated) cells. Images were captured using a phase-contrast microscope at 0 and 48 h of treatment with **11g** and **12g**. Wound widths (distance in μm) are presented in the adjacent tables.

unwinding of ds DNA upon interaction with the **11g** compound, thereby accounting for DNA intercalation [60–63]. Since there is a slight disruption in the negative band intensity at 245 nm, it is apparent that **11g** has effect on the helicity of the DNA. Similarly, CD spectrum was recorded after the addition of compound **12g** in both equal and double the concentration of the CT-DNA (Fig. 11B) also exhibited similar results. But on carefully observing the spectra, it is evident that the extent of hypochromicity with **11g** is more compared to **12g**. Similarly, the negative band at 245 nm show gradual change indicating less effect of **12g** on DNA helicity as compared to **11g**.

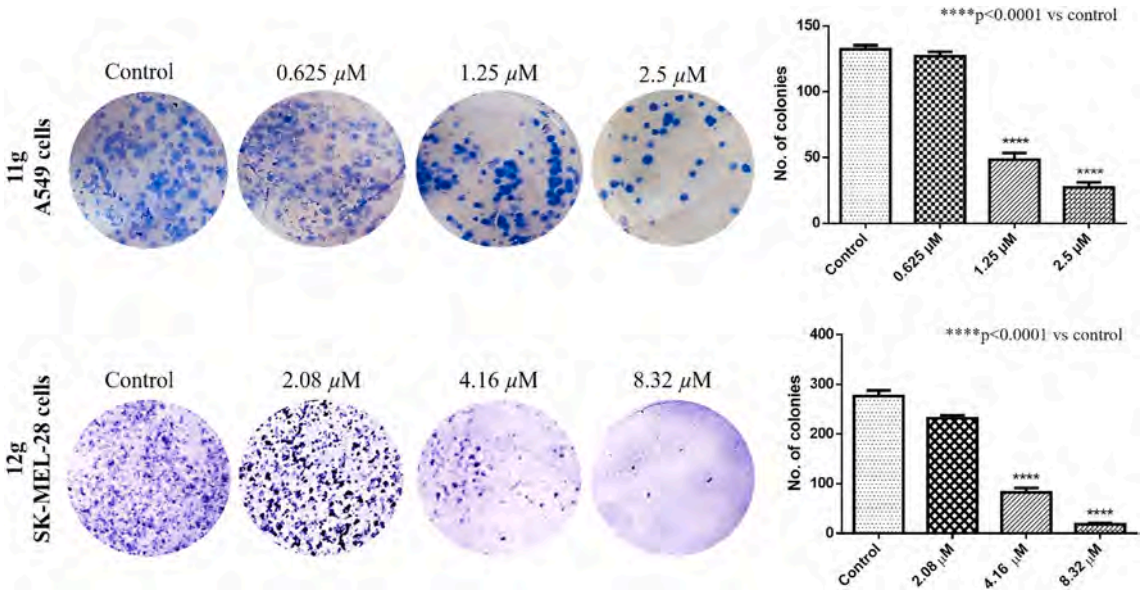

Fig. 8. Clonogenic growth inhibition assay for evaluation of the effect of varying concentrations of compound **11g** and **12g** on the colony-forming ability of A549 and SK-MEL-28 cells, respectively, after seven days.

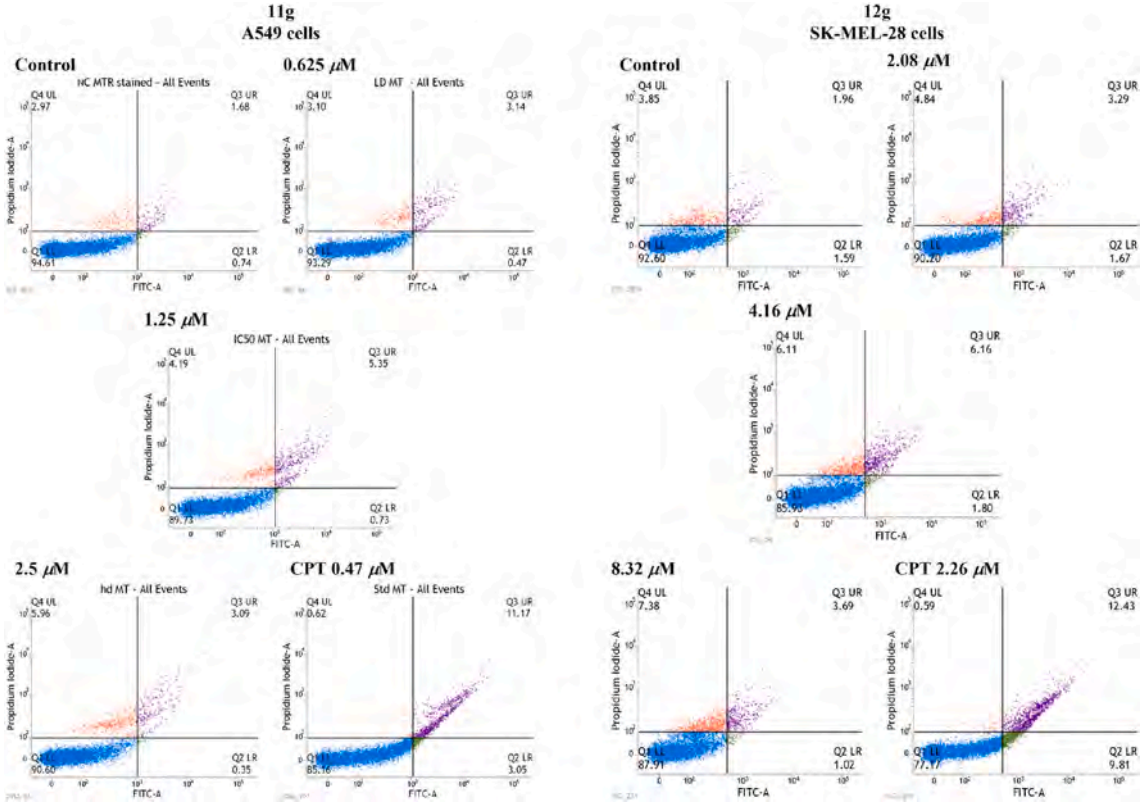

Fig. 9. Estimation of apoptotic population by Annexin V and Propidium Iodide (PI) staining by compound **11g** and **12g** in comparison with camptothecin on A549 and SK-MEL-28 cells after 48 h using BD FACSVerse™. 10,000 cells from each sample were analyzed using flow cytometry. The percentage of cells positive for Annexin V-FITC and/or Propidium iodide is reported inside the quadrants. Cells in the lower left quadrant (Q1: AV/PI): live cells; lower right quadrant (Q2: AV+/PI): early apoptotic cells; upper right quadrant (Q3: AV+/PI+): late apoptotic cells and upper left quadrant (Q4: AV/PI+): necrotic cells.

2.2.3.3. Viscosity studies. Both UV–Vis and CD spectroscopic studies indicated that both **11g** and **12g** are interacting with ds DNA and altering its conformation. But the nature of compounds interaction is not evident from the above experiments. To understand the nature of compounds interaction with ds DNA, viscosity studies were performed. Viscosity studies were carried out to further bolster the results obtained from UV–Vis, and CD spectroscopic techniques and to gain clear insights about the nature of interaction both the investigated compounds with the CT-DNA. Intercalation of a compound with the DNA results in increased relative viscosity of the DNA solution [64], whereas a negligible change in the relative viscosity is indicative of groove/surface binding [65]. The axial length of DNA double helix is known to increase

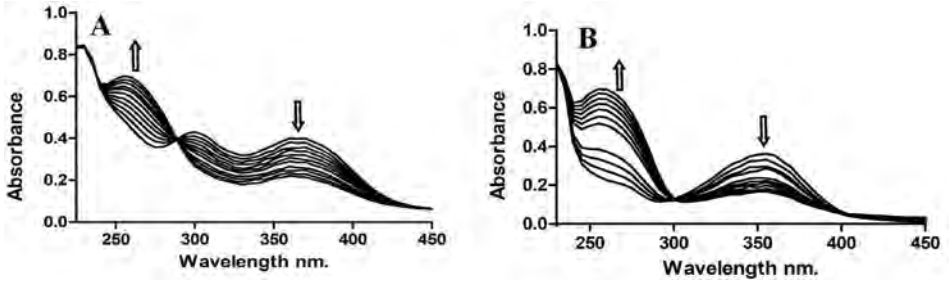

Fig. 10. UV–visible spectrum representing the titration of compound **11g** (**A**) and **12g** (**B**) with CT-DNA.

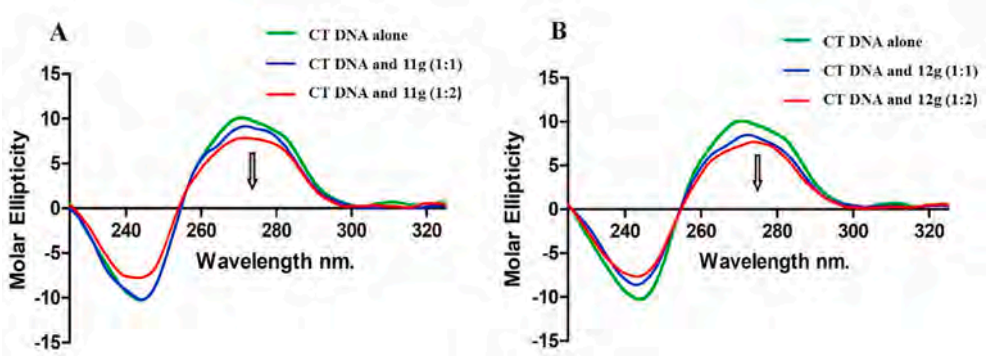

Fig. 11. CD spectra of CT-DNA (10 μM) at 10 and 20 μM of compounds **11g** (**A**) and **12g** (**B**).

to accommodate the intercalating binding agents, thereby leading to an increase in the viscosity of DNA solution.

The viscosity of DNA solution in the present study also increased with the addition of compounds **11g**, and the graph thus obtained was close to that of ethidium bromide, a well-known DNA intercalator (Fig. 12A). Relative viscosity of the CT-DNA solution after the addition of compound **12g** reduced significantly (Fig. 12B), nearing to that of a classical minor groove binder – Hoechst 33342, thus highlighting its minor groove binding nature.

2.2.4. *Topoisomerase I and II inhibition studies*

2.2.4.1. Topoisomerase I assay. Topoisomerase I makes a nick in one of the DNA strands during DNA replication and releases the superhelical tension, thereby minimizing the twisting number of DNA and transforming it into a more relaxed form. Inhibition of DNA Topo I damages the genome integrity in cancer cells. Recent years have evidenced a surged interest in Topo I inhibitors as potential anti-cancer modalities. Moreover, relatively high abundance of Topo I expressed in cancer cells compared to their normal counterparts makes Topo I a potential target for numerous clinically studied anticancer drugs. Inhibitors of Topo I are known to inhibit the DNA religation step by stabilizing and accumulating the DNA-topoisomerase cleavage complexes, thus resulting in cleaved DNA strand [66].

From the DNA binding studies, it is evident that both the compounds, **11g** and **12g** display good interaction with the double stranded DNA. Further, for better understanding of the anticancer activity of compounds **11g** and **12g**, Topo I inhibition assay is performed. When pBR322 plasmid DNA is treated with Topo I, the supercoiled pBR322 got completely converted into a relaxed form (Lane 2, Fig. 13). Whereas upon addition of **11g** (Lane 3, Fig. 13) the activity of Topo I was inhibited to a greater extent (approximately about 28% was converted to relaxed form), resulting in the formation of supercoiled form of DNA. However, the extent of inhibition was less as compared to compound **12g**, which exhibited higher of the Topo I inhibitory activity (approximately about 17% of supercoiled DNA was converted to the relaxed form). From Fig. 13 (Lane 5), it is evident that the effect of camptothecin on Topo I inhibition is greater when compared to the compounds under investigation. Gathering the results obtained from DNA binding studies and Topo I inhibition assay, together with the evidence provided by the

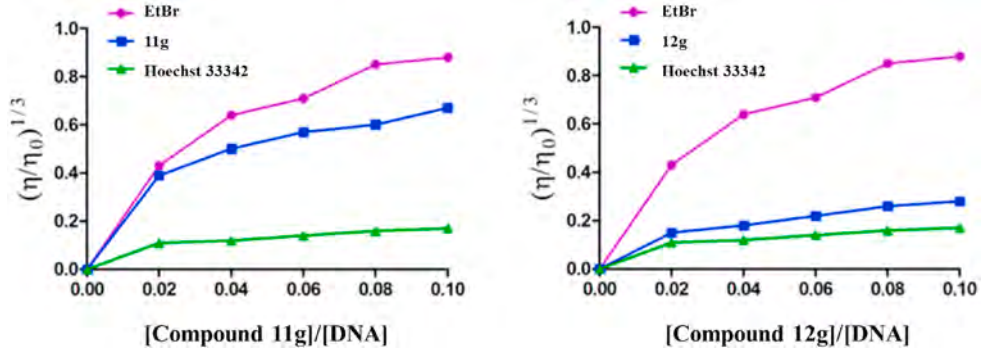

Fig. 12. Graphical representation of the relative viscosity studies of **11g** and **12g** in comparison to an intercalator (ethidium bromide, EtBr) and a potent minor groove binder (Hoechst 33342).

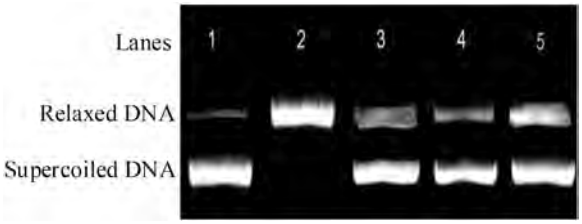

Fig. 13. Inhibition of Topo I enzyme by compounds **11g** and **12g** and their effect on transforming the supercoiled DNA (0.5 μg of pBR322 plasmid DNA) to relaxed form was studied in the presence (10 μM) and absence of the **11g** and **12g** complexes. Camptothecin (10 μM) was considered as a positive control. Lane 1: pBR322 plasmid DNA alone, Lane 2: pBR322 plasmid DNA + Topo I, Lane 3: pBR322 plasmid DNA + Topo I + **11g**, Lane 4: pBR322 plasmid DNA + Topo I + **12g**, Lane 5: pBR322 plasmid DNA + Topo I + camptothecin.

apoptotic studies, compounds **11g** and **12g** could serve as potential chemotherapeutic agents.

2.2.4.2. Topoisomerase I relaxation assay for determination of IC_{50} values. The effect of **11g** and **12g** compounds at varying concentrations (20, 40, 60 and 80 μM) on the activity of purified human Topo I was evaluated by quantitating the extent of transformation of supercoiled pBR322 plasmid DNA to relaxed form of DNA (Fig. 14). After the incubation, the plasmid DNA samples were treated with SDS and proteinase K to remove any covalently bound protein and they were resolved by running on a 1% agarose gel. The concentrations of the inhibitor that prevented 50% of the supercoiled DNA from being converted into relaxed DNA (IC_{50} values) was determined (Table 4). Camptothecin, a well-known Topo I inhibitor, was used as positive control in the assay. Enzymatic activity (relaxation of pBR322 plasmid) of Topo I was inhibited by **12g** at a concentration of 34 μM (Table 4), that is slightly less efficient than camptothecin, a positive control (IC_{50} value of 20 μM). The ability of **11g** in transforming 50% of supercoiled DNA to relaxed form (IC_{50}) was observed at around 48 μM (at a concentration that is higher than camptothecin and **12g**). From this assay, it is evident that **12g** has better ability to transform supercoiled DNA to relaxed form compared to **11g**. The IC_{50} values obtained with pBR322 plasmid DNA relaxation with **11g** and **12g** and camptothecin has been tabulated in Table 4. The IC_{50}, a function of the % inhibition value, was calculated using the formula: IC_{50} = (Conc. of tested agent × 50)/% inhibition.

2.2.4.3. Topoisomerase II inhibition assay. DNA is an important biological macromolecule involved in several molecular events in the cell and the enzyme namely Topoisomerase controls its topology. The enzyme activity is crucial for several important processes in the cell like DNA replication, transcription, segregation and recombination [67]. Though there are several kinds of topoisomerases, two main classes namely of topoisomerases are well-known. Type-I topoisomerase (Topo I) is known to make a single nick in the DNA strand and type-II topoisomerases are familiar for making nicks on both the strands of DNA. Topoisomerase II (Topo II) is a nuclear enzyme that alters the DNA topology by catalysing the DNA cleavage and relegating the phosphodiester bonds. The DNA

Table 4
Inhibitory activity of compounds **11g**, **12g** and camptothecin against hTopo I.

S. No.	Compound	IC_{50} value (μM)
1	**11g**	48
2	**12g**	34
3	camptothecin	20

strand breaks occurred due to topoisomerase enzyme activity initiates multiple recombination/repair pathways that lead to trigger cell death pathways [68]. Topo II inhibition studies are carried out using Topo II Drug Screening Kit (TG 1009, Topogen, USA). Until now, two types of topo inhibitors are well-known, they are interfacial poisons (IFPs) and catalytic inhibitory compounds (CICs). CICs interfere with the activity of the enzyme, while IFPs encourage the creation of the complexes which causes cleavage and block the relegation, resulting in formation of linear DNA. Catenated kDNA when incubated with Topo II enzyme alone under similar conditions (Lane 2, Fig. 15) resulted in complete decatenation of the DNA. Similarly, catenated DNA and Topo II enzyme (5 units) were incubated in the presence of 10 μM of **11g** and **12g** for 30 min (Lanes 3 and 4, respectively, Fig. 15) and the same concentration of etoposide (Lane 5, Fig. 15) was considered as positive control in the present experiment. From the results, it is evident that compounds **11g** and **12g** majorly showed the decatenated form of DNA as the major product, thus indicating the investigated compounds have minimal effect on Topo II activity.

2.2.5. Molecular modeling studies

2.2.5.1. Docking simulation study. Molecular docking simulation studies using Schrödinger, 2017 [69] were carried out for the compounds **11g** and **12g**, with an aim to gain additional comprehension on its binding modes against the proposed target DNA-topoisomerase I complex (PDB ID: 1K4T) [70]. Initially, co-crystal topotecan (a Topo I poison) was re-docked at the active site of Topo I to validate the docking protocol. Hydrogen bonding interactions with Arg364, Lys532 and Asp533 were displayed, as seen in Fig. 16A. Similarly, the most potent compound **11g** was docked by using the validated protocol (Fig. 16B), which revealed the hydrogen bond formation by the indolic NH with Thr718 amino acid residue of Topo I.

While, the exocyclic NH of thiazolidinone displayed hydrogen bonding with dA113D of the DNA, its *O*- and endocyclic *N*- atom formed hydrogen bond with dC112D. Likewise, **12g** was also docked (Fig. 16C)

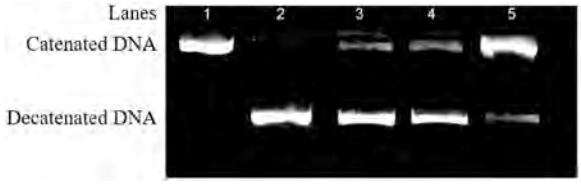

Fig. 15. DNA Topo II inhibition assay of compounds **11g** and **12g**. Lane 1: only kDNA, Lane 2: kDNA + Topo II, Lane 3: kDNA + Topo II + **11g**, Lane 4: kDNA + Topo II + **12g**, Lane 5: kDNA + Topo II + etoposide.

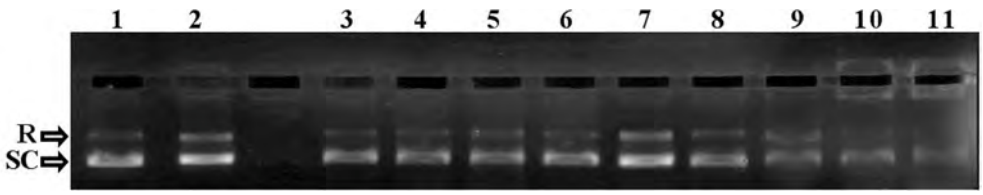

Fig. 14. DNA Topo-I inhibition assay of compounds **11g** and **12g**. Lane 1: only pBR322 plasmid DNA, Lane 2: pBR322 plasmid + DNA + Topo I, Lane 3 to 6: DNA + Topo I + **11g** at different concentration (20, 40, 60 and 80 μM), Lane 7: DNA + Topo I + camptothecin (20 μM), Lane 8 to 11: DNA + Topo I + **12g** at different concentrations (20, 40, 60 and 80 μM).

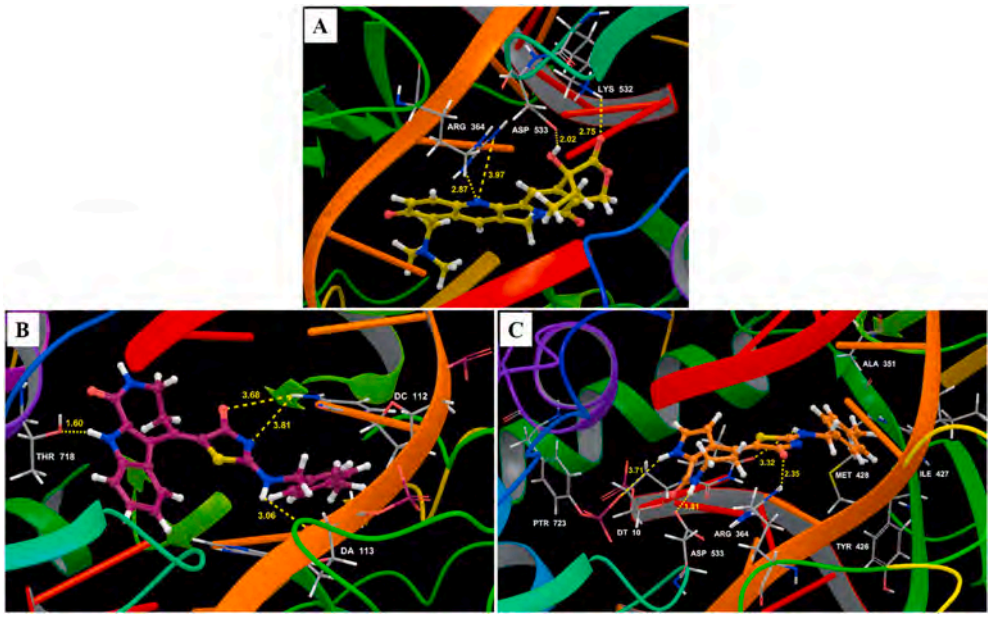

Fig. 16. (**A**), (**B**) and (**C**) represent the binding pose of co-crystal (topotecan), compounds **11g** and **12g** at the active site of DNA-topoisomerase I complex (PDB ID: 1K4T), respectively. While, the co-crystal is indicated as yellow ball and stick model, compounds **11g** is colored in purple and **12g** in orange. Hydrogen bonding interactions are indicated by yellow dotted lines.

and it was observed that the pyrrolic nitrogen formed a hydrogen bond with phosphotyrosine (Ptr732), while the amidic nitrogen bonded with dT10. Additionally, the exocyclic nitrogen atom of the thiazolidinone moiety showed hydrogen binding with Arg364 and Asp533. These results further strengthened the results corroborated by the *in vitro* DNA-binding studies, thereby, drawing the conclusion towards the DNA-minor groove binding and intercalating property of **11g** and **12g,** respectively. In addition to this, binding energy calculations were performed on the enzyme complexes with **11g** and **12g**. From the results, it was confirmed that both the ligands have good binding energies (−23.194 and −33.1185 kcal/mol, respectively), which are higher than that of the bound ligand, topotecan, (−17.330 kcal/mol). This, hence, signifies stronger binding to DNA-Topo I complex as a result of the stable ligand-protein complex formation.

2.2.5.2. In silico ADME/T studies. The chemical drug-likeness of **11g** and **12g** was assessed by using QikProp program of Schrodinger software, wherein, the ADME/T (absorption, distribution, metabolism, elimination and toxicity) parameters were calculated and depicted in Table 5. From the results obtained by performing *in silico* ADME/T prediction studies, it is evident that the compounds under investigation, **11g** and **12g**, are in accordance with the Lipinski's rule of five. Furthermore, all the physio-chemical descriptors were well within the recommended ranges.

2.2.5.3. In silico toxicity profiling. To comprehend the toxicity profile of the compounds **11g** and **12g**, 'TOPKAT' (Toxicity Prediction by Komputer Assisted Technology) module in Discovery Studio v19.1.0.18287 was employed. By developing a rigorously validated Quantitative Structure-Toxicity Relationship (QTSAR) equation, TOPKAT forecasts the rodent carcinogenicity, mutagenicity, skin & ocular irritation, the Ames test and biodegradability for given chemical structures of investigated compounds [72,73]. Table 6 depicts the *in silico* toxicity profiling results of indolo- and pyrroloazepinone-thiazolidione conjugates **11g** and **12g** in different animal models such as male and female rats and mice. Both the compounds were found to be non-mutagenic and majorly non-carcinogenic in many models. Both, **11g** and **12g** are non-degradable and do not demonstrate skin sensitization or irritancy. Other toxicity parameters such as rat oral LD_{50} and rat inhalational LC_{50},

Table 5
Drug-likeness and physico-chemical parameters of the potent compounds **11g** and **12g** predicted by QikProp [71].

S. No.	ADME/T parameters	Range or recommended values	11g	12g
1	Rule of five (Number of violations of Lipinski's rule of five)	maximum is 4	0	0
2	PSA (Van der Waals surface area of polar nitrogen and oxygen atoms)	7.0–200.0	107.621	107.575
3	SASA (Total solvent accessible surface area in square angstroms)	300.0–1000.0	714.691	649.093
4	Dipole moment	1.0–12.5	5.539	6.114
5	Molecular volume (Total solvent accessible volume)	500.0–2000.0	1261.817	1124.729
6	Donor HB	0.0–6.0	3	3
7	Acceptor HB	2.0–20.0	6.5	6.5
8	QPlogKhsa (Prediction of binding to human serum albumin)	−1.5–1.5	0.544	0.215
9	QPlogPo/w (Predicted octanol/water partition coefficient)	−2.0–6.5	3.328	2.405
10	QPpolrz (Predicted polarizability in cubic angstroms)	13.0–70.0	45.493	39.299
11	QPlogBB (Predicted brain/blood partition coefficient)	−3.0–1.2	−1.531	−1.484
12	QPlogKp (Predicted skin permeability)	−8.0–−1.0	−3.458	−3.783
13	QPlogHERG (Predicted IC_{50} value for blockage of HERG K^+ channels)	concern below −5	−6.463	−5.857
14	QPPCaco (Predicted apparent Caco-2 cell permeability in nm/sec)	<25 is poor, >500 is great	184.828	171.255
15	POA (Predicted human oral absorption on 0–100% scale)	<25% is poor, >80% is high	87.001	81.007

Table 6
Probability values of different toxicity models forecasted by TOPKAT for **11g** and **12g**.

TOPKAT model	11g	12g
Mouse_Female_NTP	Non-Carcinogen (−2.69)	Non-Carcinogen (−2.07)
Mouse_Male_NTP	Non-Carcinogen (−8.13)	Non-Carcinogen (−7.73)
Rat_Female_NTP	Non-Carcinogen (−1.92)	Non-Carcinogen (−3.60)
Rat_Male_NTP	Carcinogen (1.57)	Non-Carcinogen (0.72)
Mouse_Female_FDA	Non-Carcinogen	Non-Carcinogen
Mouse_Male_FDA	Non-Carcinogen	Non-Carcinogen
Rat_Female_FDA	Single-carcinogen	Non-Carcinogen
Rat_Male_FDA	Non-Carcinogen	Non-Carcinogen
Mouse_Female_FDA_None_vs_Carcinogen	Non-Carcinogen (−5.82)	Non-Carcinogen (−5.14)
Mouse_Male_FDA_None_vs_Carcinogen	Non-Carcinogen (−5.0)	Non-Carcinogen (−4.39)
Rat_Female_FDA_None_vs_Carcinogen	Carcinogen (−0.67)	Non-Carcinogen (−4.02)
Rat_Female_FDA_Single_vs_Multiple	Single-carcinogen (−0.2)	–
Rat_Male_FDA_None_vs_Carcinogen	Non-Carcinogen (−0.48)	Non-Carcinogen (−3.64)
WOE_Prediction	Non-Carcinogen (−4.74)	Non-Carcinogen (−6.23)
Carcinogenic_Potency_TD_{50}_Mouse (mg/kg_body_weight/day)	5.65	10.78
Carcinogenic_Potency_TD_{50}_Rat (mg/kg_body_weight/day)	5.78	7.62
Ames_Prediction	Non-Mutagen (−3.48)	Non-Mutagen (−6.22)
DTP_Prediction	Non-Toxic (−2.43)	Non-Toxic (−3.38)
Rat_Oral_LD_{50} (mg/kg_body_weight)	4322.18	3505.09
Rat_Maximum_Tolerated_Dose_Feed (mg/kg_body_weight)	82.51	82.26
Rat_Maximum_Tolerated_Dose_Gavage (mg/kg_body_weight)	15.03	31.3
Rat_Inhalational_LC_{50} (mg/m^3/h)	932.66	857.49
Chronic_LOAEL (mg/kg_body_weight)	69.15	51.15
Skin_Irritancy	None	None
Skin_Irritancy_None_vs_Irritant	Non-irritant (−0.97)	Non-irritant (−0.96)
Skin_Sensitization	None	None
Skin_Sensitization_None_vs_Sensitizer	Non-irritant (−5.79)	Non-irritant (−2.99)
Ocular_Irritancy	Mild	Mild
Ocular_Irritancy_None_vs_Irritant	Irritant (1.81)	Irritant (1.42)
Ocular_Irritancy_Mild_vs_Moderate_Severe	Mild (−1.41)	Mild (−1.06)
Aerobic_Biodegradability	Non-Degradable (−9.12)	Non-Degradable (−5.29)
Fathead_Minnow_LC_{50} (mg/L)	1.14	7.18
Daphnia_EC_{50} (mg/L)	0.21	0.65

rat maximum tolerated dose are summarized in Table 6. Results thus collated are indicative of the safety of the examined compounds' safety in many animal models with minimal toxicological profile.

2.3. Conclusion

In conclusion, a $TiCl_4$-mediated modified Knoevenagel condensation reaction for the synthesis of new thiazolidinone-based indolo-/pyrroloazepinone conjugates was accomplished *via* molecular hybridization and evaluated for their antiproliferative potential and Topo I and II inhibition. Among these new conjugates, **11g** was found to be the most potent compound exhibiting IC_{50} value of 1.24 μM in A549 (lung cancer cells) and 3.02–10.91 μM in the other cancer cell lines. Additionally, it showed 43-fold selectivity towards the cancer cell line (A549) as compared to normal rat kidney epithelial cells. In the pyrroloazepinone-based conjugates, **12g** was found to be the most active in SK-MEL-28 cells. Structure-activity relationship (SAR) was constructed based on the preliminary *in vitro* cytotoxicity results. Further, apoptotic studies including morphological observations, DAPI nucleic acid, AO/EB and DCFDA staining assays showed that both the investigated compounds induced apoptosis in the cancer cell lines. **11g** and **12g** also demonstrated concentration-dependent inhibition in the cell migration. Clonogenic assay was performed to evaluate the cell growth inhibitory potential of the lead compounds. UV–Visible, circular dichroism spectroscopic and viscosity studies were employed to examine the mode of DNA binding interactions. It was revealed that **11g** may align between the base pairs of the DNA, thus, demonstrating intercalative mode of binding, whereas **12g** arranges itself along the minor groove. Topo I and Topo II inhibition assays further threw light on the possible mode of action of these compounds in exhibiting their anticancer activity. Further, the biological assays like wound healing, apoptosis induction and its quantification, cell growth inhibition and ROS generation assay, support the role of these molecules in carrying out the anticancer activity among cancer cells. Moreover, the *in vitro* results were espoused by molecular modeling studies. The drug-likeliness of **11g** and **12g** were evaluated by the *in silico* ADME/T profiling using Qikprop. To assess the toxicity profiling of these compounds in animal models, *in silico* prediction studies were carried out utilizing TOPKAT tool. Thus, with the procured experimental data, 4-thiazolidinone-based indolo-/pyrroloazepinone conjugates can be identified as a novel class of compounds with significant cytotoxicity and DNA-Topo I inhibitory activity.

2.4. Experimental section

2.4.1. General procedures

Reagents and solvents were purchased from commercial sources. All the reactions were monitored routinely by thin layer chromatography (TLC) performed on MERCK silica gel 60-F254 (0.5 mm) pre-coated aluminum plates and visualized using ultraviolet light or by treatment with iodine or anisaldehyde dip. Column chromatography was performed by using silica gel (60–120). Evaporation of the solvents was performed under reduced pressure by using a rotary evaporator below 45 °C. ^{1}H and ^{13}C NMR spectra were recorded with a Bruker 500 MHz instrument in $CDCl_3$ or [d_6] DMSO solvent with tetramethylsilane as the internal standard. Chemical shifts for ^{1}H and ^{13}C are reported in parts per million (ppm) downfield from tetramethylsilane. Spin multiplicities are described as s (singlet), brs (broad singlet), d (doublet), t (triplet), q (quartet) and m (multiplet). Coupling constant (*J*) values are reported in hertz (Hz). HRMS was performed with an Agilent QTOF mass spectrometer 6540 series instrument. Melting points were determined using an electrothermal digital melting point apparatus IA9100. Infrared spectra (IR) were recorded on a PerkinElmer 1600 series FTIR spectrometer. The names of all the compounds given in the experimental section were taken from ChemBioDraw Ultra, Version 14.0.

2.4.2. Chemistry

*2.4.2.1. General procedure for N-methylated indolo/pyrroloazepinone (**5–6**).* To an acetonitrile solution of indolo/pyrroloazepinone **3**/**4** was added K_2CO_3 (3.5 equiv.) and stirred for 15 min, after which CH_3I (3 equiv.) was added and refluxed till completion of the reaction. Upon completion, the solvent was evaporated under vacuum and water was added followed by extraction with ethyl acetate. *N*-methylated indolo/pyrroloazepinone (**5**/**6**) was obtained as solid (83 and 84%, respectively).

*2.4.2.2. General procedure for benzyl/phenethyl thiazolidinones (**10**).* To a solution of different benzyl amines **7** (1 equiv.) in DMF (2–3 mL) maintained at 0 °C, chloroacetyl chloride **8** (1.5 equiv.) was added dropwise with constant stirring. The reaction mixture was then brought to rt and stirred for 2 h. To the reaction mixture, was added crushed ice and shaken vigorously. To this, EtOAc was added, and extraction was carried out. The organic layer was further concentrated under vacuum to obtain respective *N*-benzyl-2-chloroacetamide **9** as solid, which was filtered, exhaustively washed with water and dried under vacuum. The mixture of *N*-benzyl-2-chloroacetamide **9** (1 equiv.) and ammonium thiocyanate (2 equiv.) in ethanol (2–4 mL) was refluxed overnight. After completion of the reaction, solid thus obtained was separated by filtration and recrystallized from ethanol to give the corresponding benzyl/phenethyl thiazolidinones (**10**) in good to excellent yields (72–95%).

*2.4.2.3. (2E,5Z)-2-(benzyl/phenethylimino)-5-(1-oxo-1,3,4,10-tetrahydroazepino [3,4-b]indol-5(2H)-ylidene)thiazolidin-4-one (**11a-l**).* The titled compound was obtained by taking respective (*E*)-2-(benzyl/phenethylimino)thiazolidin-4-ones (**10a-n**, 1.5 equiv.) and 3,4-dihydroazepino [3,4-*b*]indole-1,5(2*H*,10*H*)-diones (**5a-b**, 1 mmol) in the reaction vessel with dry THF maintained under N_2 atmosphere at 0 °C, to which $TiCl_4$ (99%, 1 equiv.) was added dropwise and allowed to stir for 30 min followed by slow addition (over two fractions) of pyridine (6 equiv.). The reaction mixture was allowed to stir for 24 h to yield the desired final compounds **11a-l** in a good to excellent yields (81–95%).

*2.4.2.4. (2E,5Z)-2-(benzylimino)-5-(1-oxo-1,3,4,10-tetrahydroazepino [3,4-b]indol-5(2H)-ylidene)thiazolidin-4-one (**11a**).* Pale yellow solid; 82% yield; mp: 249–251 °C; FT-IR (cm^{-1}): 3294, 3229, 3072, 2864, 1688, 1651, 159, 1582, 1569, 1528, 1394, 1326, 1299, 1251, 1145, 1090, 1046, 940, 742, 694, 489; ^{1}H NMR (500 MHz, DMSO-d_6): δ 12.38 (s, 1H), 9.19 (s, 1H), 8.32 (s, 1H), 7.53–7.51 (m, 1H), 7.49 (d, J = 7.9 Hz, 1H), 7.35 (s, 1H), 7.34 (s, 2H), 7.32–7.29 (m, 1H), 7.29–7.26 (m, 1H), 7.21–7.19 (m, 2H), 4.90 (s, 2H), 3.36–3.34 (m, 3H), 3.31–3.28 (m, 1H). ^{13}C NMR (125 MHz, DMSO-d_6): δ 165.4, 165.4, 153.8, 140.1, 137.2, 136.5, 131.9, 128.9, 128.1, 127.7, 124.6, 123.1, 122.8, 120.8, 120.7, 115.5, 113.4, 44.4, 39.6, 39.2. HRMS (ESI): *m/z* calcd for $C_{22}H_{18}N_4O_2S$ 403.1223 found 403.1219 $[M+H]^+$.

*2.4.2.5. (2E,5Z)-2-((3-chlorobenzyl)imino)-5-(1-oxo-1,3,4,10-tetrahydroazepino [3,4-b]indol-5(2H)-ylidene)thiazolidin-4-one (**11b**).* Beige solid; 81% yield; mp: 287–289 °C; FT-IR (cm^{-1}): 3294, 3215, 3079, 1722, 1671, 1616, 1565, 1469, 1387, 1350, 1326, 1305, 1254, 1145, 1094, 1039, 947, 752, 677, 608, 537, 485; ^{1}H NMR (500 MHz, DMSO-d_6): δ 12.41 (s, 1H), 9.23 (s, 1H), 8.35 (s, 1H), 7.51 (t, J = 7.6 Hz, 2H), 7.42–7.40 (m, 1H), 7.39 (s, 1H), 7.37–7.36 (m, 1H), 7.31 (t, J = 7.7 Hz, 2H), 7.19 (t, J = 7.6 Hz, 1H), 4.89 (s, 2H), 3.33–3.28 (m, 4H). ^{13}C NMR (125 MHz, DMSO-d_6): δ 165.4, 165.4, 153.8, 140.4, 139.7, 136.5, 133.4, 131.9, 130.9, 128.1, 127.8, 126.9, 124.6, 123.1, 122.8, 120.7, 120.6, 115.4, 113.4, 43.9, 39.5, 39.1. HRMS (ESI): *m/z* calcd for $C_{22}H_{17}ClN_4O_2S$ 437.0834 found 437.0832 $[M+H]^+$ and 439.0808 $[M+2]^+$.

*2.4.2.6. (2E,5Z)-2-((4-fluorobenzyl)imino)-5-(1-oxo-1,3,4,10-tetrahydroazepino [3,4-b]indol-5(2H)-ylidene)thiazolidin-4-one (**11c**).* Pale yellow solid; 76% yield; mp: 251–253 °C; FT-IR (cm^{-1}): 3219, 3065, 2932, 1685, 1651, 1613, 1565, 1510, 1473, 1425, 1384, 1329, 1299, 1220, 1159, 1097, 936, 827, 748, 622, 571, 482; ^{1}H NMR (500 MHz, DMSO-d_6): δ 12.38 (s, 1H), 9.21 (s, 1H), 8.32 (t, J = 5.6 Hz, 1H), 7.51 (d, J = 8.2 Hz, 1H), 7.47–7.40 (m, 1H), 7.41–7.38 (m, 2H), 7.32–7.29 (m, 1H), 7.20–7.15 (m, 3H), 4.87 (s, 2H), 3.34 (d, J = 2.6 Hz, 1H), 3.31–3.28 (m, 3H). ^{13}C NMR (125 MHz, DMSO-d_6): δ 164.8, 161.4 (d, J_{CF} = 243.1, Hz), 139.8, 135.9, 132.9, 131.3, 129.9 (d, J_{CF} = 129.86,1 Hz), 124.0, 122.4 (d, J_{CF} = 24.6 Hz), 120.1, 120.1, 115.1, 115.0, 114.9, 112.8, 43.1, 39.1, 38.6. HRMS (ESI): *m/z* calcd for $C_{22}H_{17}FN_4O_2S$ 421.1129 found 421.1122 $[M+H]^+$.

*2.4.2.7. (2E,5Z)-2-((3-methoxybenzyl)imino)-5-(1-oxo-1,3,4,10-tetrahydroazepino [3,4-b]indol-5(2H)-ylidene)thiazolidin-4-one (**11d**).* Pale yellow solid; 92% yield; mp: 270–272 °C; FT-IR (cm^{-1}): 3280, 3239, 2939, 2835, 1685, 1651, 1610, 1510, 1398, 1357, 1329, 1244, 1179, 1138, 1032, 827, 748, 615, 489; ^{1}H NMR (500 MHz, DMSO-d_6): δ 12.37 (s, 1H), 9.18 (s, 1H), 8.31 (t, J = 5.5 Hz, 1H), 7.51 (d, J = 8.2 Hz, 1H), 7.46 (d, J = 8.2 Hz, 1H), 7.30 (dd, J = 6.4, 2.4 Hz, 3H), 7.20–7.17 (m, 1H), 6.90 (dd, J = 6.4, 2.3 Hz, 2H), 4.82 (s, 2H), 3.74 (s, 3H), 3.73–3.68 (m, 2H), 3.30–3.27 (m, 2H). ^{13}C NMR (125 MHz, DMSO-d_6): δ 165.4, 165.4, 159.0, 153.8, 140.0, 136.5, 131.8, 129.9, 129.3, 124.6, 123.0, 122.8, 120.8, 120.7, 115.5, 114.2, 113.4, 55.5, 43.8, 39.5, 39.1. HRMS (ESI): *m/z* calcd for $C_{23}H_{20}N_4O_3S$ 433.1329 found 433.1322 $[M+H]^+$.

*2.4.2.8. (2E,5Z)-2-((3,4-dimethoxybenzyl)imino)-5-(1-oxo-1,3,4,10-tetrahydroazepino [3,4-b]indol-5(2H)-ylidene)thiazolidin-4-one (**11e**).* Pale yellow solid; 95% yield; mp: 270–272 °C; FT-IR (cm^{-1}): 3280, 3205, 2942, 2836, 1712, 1685, 1651, 1610, 1510, 1401, 1357, 1329, 1343, 1329, 1247, 1179, 1141, 1032, 830, 752, 612, 516, 489; ^{1}H NMR (500 MHz, DMSO-d_6): δ 12.39 (s, 1H), 9.15 (s, 1H), 8.34 (t, J = 5.6 Hz, 1H), 7.51 (d, J = 8.2 Hz, 1H), 7.43 (d, J = 8.2 Hz, 1H), 7.32–7.29 (m, 1H), 7.21–7.18 (m, 1H), 6.88 (d, J = 8.2 Hz, 1H), 6.77–6.72 (m, 2H), 3.74 (s, 3H), 3.73 (s, 3H), 3.38 (t, J = 4.5 Hz, 2H), 3.30–3.30 (m, 2H). ^{13}C NMR (125 MHz, DMSO-d_6): δ 165.8, 163.9, 153.7, 142.1, 136.2, 132.4, 130.0, 128.9, 127.0, 123.8, 122.5, 117.5, 109.5, 60.2, 43.7, 39.5, 36.8. HRMS (ESI): *m/z* calcd for $C_{24}H_{22}N_4O_2S$ 463.1435 found 463.1424 $[M+H]^+$.

*2.4.2.9. (2E,5Z)-2-((4-chlorobenzyl)imino)-5-(1-oxo-1,3,4,10-tetrahydroazepino [3,4-b]indol-5(2H)-ylidene)thiazolidin-4-one (**11f**).* Yellow solid; 79% yield; mp: 140–142 °C; FT-IR (cm^{-1}): 3260, 3065, 2925, 2850, 1692, 1651, 616, 1562, 1521, 1490, 1387, 1329, 1254, 1299, 1145, 1090, 1053, 936, 796, 748, 612, 561; ^{1}H NMR (500 MHz, DMSO-d_6): δ 12.40 (s, 1H), 9.22 (s, 1H), 8.34 (t, J = 5.5 Hz, 1H), 7.52 (d, J = 8.2 Hz, 1H), 7.49 (d, J = 8.2 Hz, 1H), 7.42–7.40 (m, 2H), 7.36 (dd, J = 5.9, 2.6 Hz, 2H), 7.31 (t, J = 7.6 Hz, 1H), 7.19 (t, J = 7.5 Hz, 1H), 4.88 (s, 2H), 3.38–3.35 (m, 1H), 3.32–3.30 (m, 3H). ^{13}C NMR (125 MHz, DMSO-d_6): δ 165.4, 136.5, 136.2, 132.4, 131.9, 130.1, 129.5, 128.9, 128.6, 124.6, 123.1, 122.8, 120.7, 115.4, 113.4, 43.7, 41.9, 39.1. HRMS (ESI): *m/z* calcd for $C_{22}H_{17}ClN_4O_2S$ 437.0834 found 437.0831 $[M+H]^+$ and 439.0805 $[M+2]^+$.

*2.4.2.10. (2E,5Z)-2-((4-methylbenzyl)imino)-5-(1-oxo-1,3,4,10-tetrahydroazepino [3,4-b]indol-5(2H)-ylidene)thiazolidin-4-one (**11g**).* Light brown; 91% yield; mp: 262–264 °C; FT-IR (cm^{-1}): 3284, 3222, 3161, 3051, 2905, 2874, 1692, 1640, 1603, 1514, 1415, 1469, 1384, 1333, 1309, 1155, 960, 745, 622, 565, 492; ^{1}H NMR (500 MHz, DMSO-d_6): δ 12.39 (s, 1H), 9.19 (s, 1H), 8.33 (t, J = 5.5 Hz, 1H), 7.51 (d, J = 8.2 Hz, 1H), 7.47 (d, J = 8.1 Hz, 1H), 7.32–7.29 (m, 1H), 7.24 (d, J = 8.0 Hz, 2H), 7.20–7.17 (m, 2H), 7.14 (d, J = 7.9 Hz, 2H), 4.84 (s, 2H), 3.33–3.25 (m, 4H), 2.28 (s, 3H). ^{13}C NMR (125 MHz, DMSO-d_6): δ 165.4, 153.7, 140.0, 136.9, 136.5, 134.3, 131.9, 129.4, 128.3, 124.6, 123.1, 122.8, 120.8, 120.7, 115.5, 113.4, 44.1, 39.5, 39.2, 21.2. HRMS (ESI): *m/z*

calcd for $C_{23}H_{20}N_4O_2S$ 417.1380 found 417.1372 $[M+H]^+$.

*2.4.2.11. (2E,5Z)-2-((4-(tert-butyl)benzyl)imino)-5-(1-oxo-1,3,4,10-tetrahydroazepino [3,4-b]indol-5(2H)-ylidene)thiazolidin-4-one (**11h**).* Pale yellow; 92% yield; mp: 276–278 °C; FT-IR (cm^{-1}) 3294, 3226, 3069, 2959, 2918, 2870, 1692, 1651, 1616, 1565, 1521, 1473, 1425, 1387, 1329, 1148, 1111, 940, 748; ^{1}H NMR (500 MHz, DMSO-d_6): δ 12.39 (s, 1H), 9.19 (s, 1H), 8.33 (t, $J = 5.5$ Hz, 1H), 7.51 (d, $J = 8.2$ Hz, 1H), 7.47 (d, $J = 8.1$ Hz, 1H), 7.36 (d, $J = 8.4$ Hz, 2H), 7.32–7.29 (m, 1H), 7.27 (d, $J = 8.4$ Hz, 2H), 7.19 (t, $J = 7.5$ Hz, 1H), 4.85 (s, 2H), 3.31–3.30 (m, 4H), 1.27 (s, 9H). ^{13}C NMR (125 MHz, DMSO-d_6): δ 165.4, 165.4, 153.7, 150.1, 140.0, 136.5, 134.3, 131.8, 128.0, 125.6, 124.6, 123.1, 122.8, 120.8, 120.7, 115.5, 113.4, 44.0, 39.5, 39.1, 34.7, 31.6. HRMS (ESI): *m/z* calcd for $C_{26}H_{26}N_4O_2S$ 459.1849 found 459.1841 $[M+H]^+$.

*2.4.2.12. (2E,5Z)-2-((benzo[d] [1,3]dioxol-5-ylmethyl)imino)-5-(1-oxo-1,3,4,10-tetrahydroazepino [3,4-b]indol-5(2H)-ylidene)thiazolidin-4-one (**11i**).* Pale orange; 87% yield; mp: 241–243 °C; FT-IR (cm^{-1}): 3399, 3188, 3072, 2926, 2854, 1683, 1666, 1612, 1568, 1527, 1472, 1398, 1329, 1221, 1118, 1047, 887, 744, 683, 674, 543, 495; ^{1}H NMR (500 MHz, DMSO-d_6): δ 12.08 (s, 1H), 9.28 (s, 1H), 8.01 (t, $J = 5.1$ Hz, 1H), 7.31 (dd, $J = 5.6$, 2.0 Hz, 2H), 7.29 (s, 1H), 7.22–7.21 (m, 2H), 7.07 (t, $J = 2.8$ Hz, 2H), 6.48 (s, 2H), 3.45–3.43 (m, 2H), 3.24 (s, 2H), 2.87 (dd, $J = 8.6$, 6.8 Hz, 2H)·^{13}C NMR (125 MHz, DMSO-d_6): δ 165.4, 165.4, 161.3, 153.8, 147.6, 147.0, 140.1, 136.5, 131.8, 131.0, 124.6, 122.8, 122.0, 120.8, 120.7, 115.5, 113.4, 109.1, 108.6, 101.4, 44.1, 39.5, 39.1. HRMS (ESI): *m/z* calcd for $C_{23}H_{18}N_4O_4S$ 447.1122 found 447.1114 $[M+H]^+$.

*2.4.2.13. (2E,5Z)-2-(benzylimino)-5-(10-methyl-1-oxo-1,3,4,10-tetrahydroazepino [3,4-b]indol-5(2H)-ylidene)thiazolidin-4-one (**11j**).* Light brown; 94% yield; mp: 228–230 °C; FT-IR (cm^{-1}): 3362, 3260, 1688, 1657, 1616, 1582, 1510, 1500, 1432, 1394, 1305, 1152, 1042, 882, 742, 697, 660, 608, 540, 492; ^{1}H NMR (500 MHz, DMSO-d_6): δ 9.24 (s, 1H), 8.46 (t, $J = 6.0$ Hz, 1H), 7.67 (d, $J = 8.4$ Hz, 1H), 7.50 (d, $J = 8.1$ Hz, 1H), 7.40–7.37 (m, 1H), 7.35 (s, 2H), 7.34 (s, 2H), 7.28 (d, $J = 4.7$ Hz, 1H), 7.24 (t, $J = 7.5$ Hz, 1H), 4.90 (s, 2H), 3.97 (s, 3H), 3.27–3.21 (m, 2H), 3.12–3.07 (m, 2H). ^{13}C NMR (125 MHz, DMSO-d_6): δ 165.3, 164.8, 153.6, 139.6, 138.1, 137.2, 131.9, 128.9, 128.1, 127.7, 124.6, 122.9, 121.9, 121.7, 121.1, 115.4, 111.7, 44.4, 39.5, 38.7, 31.8. HRMS (ESI): *m/z* calcd for $C_{23}H_{20}N_4O_2S$ 417.1380 found 417.1370 $[M+H]^+$.

*2.4.2.14. (2E,5Z)-2-((4-methoxyphenethyl)imino)-5-(1-oxo-1,3,4,10-tetrahydroazepino [3,4-b]indol-5(2H)-ylidene)thiazolidin-4-one (**11k**).* Pale orange; 92% yield; mp: 240–242 °C; FT-IR (cm^{-1}): 3280, 3205, 2942, 2836, 1712, 1685, 1651, 1610, 1510, 1401, 1357, 1343, 1329, 1247, 1179, 1046, 1032, 830, 752, 612, 516, 489; ^{1}H NMR (500 MHz, DMSO-d_6): δ 12.38 (s, 1H), 9.14 (s, 1H), 8.33 (t, $J = 5.6$ Hz, 1H), 7.51 (d, $J = 8.3$ Hz, 1H), 7.45 (d, $J = 8.8$ Hz, 1H), 7.30 (ddd, $J = 8.2$, 6.9, 1.1 Hz, 1H), 7.19 (ddd, $J = 8.2$, 6.9, 1.1 Hz, 1H), 7.15 (d, $J = 8.7$ Hz, 2H), 6.88 (d, $J = 8.7$ Hz, 2H), 3.88–3.84 (m, 1H), 3.74 (s, 2H), 3.73–3.72 (m, 2H), 2.82 (dd, $J = 8.5$, 6.8 Hz, 2H). ^{13}C NMR (125 MHz, DMSO-d_6): δ 165.4, 158.3, 136.5, 131.8, 130.1, 124.6, 123.0, 120.6, 115.5, 114.9, 113.4, 60.2, 55.5, 42.7, 32.3, 21.2. HRMS (ESI): *m/z* calcd for $C_{24}H_{22}N_4O_3S$ 447.1485 found 447.1496 $[M+H]^+$.

*2.4.2.15. (2E,5Z)-2-((4-fluorophenethyl)imino)-5-(1-oxo-1,3,4,10-tetrahydroazepino [3,4-b]indol-5(2H)-ylidene)thiazolidin-4-one (**11l**).* Beige; 87% yield; mp: 230–232 °C; FT-IR (cm^{-1}): 3397, 3270, 3219, 1681, 651, 1603, 1586, 1569, 1510, 1432, 1394, 1357, 1329, 1220, 1141, 1049, 830, 745, 554, 475; ^{1}H NMR (500 MHz, DMSO-d_6): δ 12.40 (s, 1H), 9.16 (s, 1H), 8.35 (t, $J = 5.6$ Hz, 1H), 7.52 (d, $J = 8.2$ Hz, 1H), 7.44 (d, $J = 8.1$ Hz, 1H), 7.31 (t, $J = 7.5$ Hz, 1H), 7.26 (d, $J = 3.0$ Hz, 1H), 7.20 (t, $J = 7.6$ Hz, 1H), 7.15–7.12 (m, 3H), 3.91–3.88 (m, 4H), 3.29 (t, $J = 5.8$ Hz, 2H), 2.91–2.88 (m, 2H). ^{13}C NMR (125 MHz, DMSO-d_6): δ 165.4, 165.2, 161.4 (d, $J_{CF} = 241.8$ Hz), 153.6, 139.6, 136.5, 135.1, 131.8, 130.9 (d, $J_{CF} = 7.9$ Hz), 124.6, 123.0, 122.8, 120.9, 120.6, 115.7, 115.5, 113.4, 42.4, 39.5, 39.2, 32.3. HRMS (ESI): *m/z* calcd for $C_{23}H_{19}FN_4O_2S$ 435.1286 found 435.1268 $[M+H]^+$

*2.4.2.16. (2E,5Z)-2-(benzylimino)-5-(8-oxo-5,6,7,8-tetrahydropyrrolo [2,3-c]azepin-4(1H)-ylidene)thiazolidin-4-one (**12a**).* Pale orange; 84% yield; mp: 232–234 °C; FT-IR (cm^{-1}): 3294, 3185, 3065, 2942, 2908, 1698, 1651, 1565, 1613, 1469, 1422, 1381, 1333, 1268, 1244, 1141, 1090, 776, 742, 6294, 629, 537, 496; ^{1}H NMR (500 MHz, DMSO-d_6): δ 12.10 (s, 1H), 9.33 (s, 1H), 8.02 (t, $J = 5.1$ Hz, 1H), 7.34–7.33 (m, 1H), 7.31 (d, $J = 3.3$ Hz, 2H), 7.30–7.27 (m, 1H), 7.27–7.24 (m, 1H), 7.08 (t, $J = 2.8$ Hz, 1H), 6.51 (t, $J = 2.6$ Hz, 1H), 4.88 (s, 2H), 3.49–3.47 (m, 2H), 3.26–3.23 (m, 2H). ^{13}C NMR (125 MHz, DMSO-d_6): δ 165.8, 163.8, 153.7, 141.8, 137.2, 128.8, 128.0, 127.7, 127.0, 123.8, 122.4, 117.5, 109.5, 44.3, 40.6, 36.6. HRMS (ESI): *m/z* calcd for $C_{18}H_{16}N_4O_2S$ 353.1067 found 353.1062 $[M+H]^+$.

*2.4.2.17. (2E,5Z)-2-((4-methoxybenzyl)imino)-5-(8-oxo-5,6,7,8-tetrahydropyrrolo [2,3-c]azepin-4(1H)-ylidene)thiazolidin-4-one (**12b**).* Pale yellow; 97% yield; mp: 244–246 °C; FT-IR (cm^{-1}): 3256, 3209, 3058, 2922, 1695, 1661, 1634, 1589, 1565, 1517, 1473, 1398, 1340, 1152, 899, 766, 748, 697, 489; ^{1}H NMR (500 MHz, DMSO-d_6): δ 12.10 (s, 1H), 9.33 (s, 1H), 8.03 (t, $J = 4.7$ Hz, 1H), 7.27 (d, $J = 8.5$ Hz, 2H), 7.07 (t, $J = 2.7$ Hz, 1H), 6.88 (d, $J = 8.6$ Hz, 2H), 6.49 (t, $J = 2.3$ Hz, 1H), 4.81 (s, 2H), 3.73 (s, 3H), 3.57–3.43 (m, 2H), 3.25 (dd, $J = 10.0$, 4.7 Hz, 2H). ^{13}C NMR (125 MHz, DMSO-d_6): δ 165.8, 163.8, 159.0, 129.8, 129.2, 127.0, 123.8, 122.4, 117.6, 114.2, 109.6, 55.6, 43.8, 40.6, 36.6. HRMS (ESI): *m/z* calcd for $C_{19}H_{18}N_4O_3S$ 383.1172 found 383.0976 $[M+H]^+$.

*2.4.2.18. (2E,5Z)-5-(8-oxo-5,6,7,8-tetrahydropyrrolo [2,3-c]azepin-4(1H)-ylidene)-2-((4-(trifluoromethyl)benzyl)imino)thiazolidin-4-one (**12c**).* Cream; 86% yield; mp: 214–216 °C; FT-IR (cm^{-1}): 3233, 3164, 3065, 2952, 2911, 1702, 1644, 1610, 1565, 1469, 1425, 1381, 1326, 1312, 1268, 1244, 1145, 1128, 1104, 1066, 1022, 933, 776, 643; ^{1}H NMR (500 MHz, DMSO-d_6): δ 12.11 (s, 1H), 9.36 (s, 1H), 8.03 (t, $J = 5.2$ Hz, 1H), 7.70 (d, $J = 8.5$ Hz, 2H), 7.51 (d, $J = 8.2$ Hz, 2H), 7.08 (t, $J = 2.9$ Hz, 1H), 6.51 (t, $J = 2.6$ Hz, 1H), 4.97 (s, 2H), 3.49–3.47 (m, 2H), 3.27–3.24 (m, 2H). ^{13}C NMR (125 MHz, DMSO-d_6): δ 165.8, 163.8, 153.7, 142.2, 141.9, 141.9, 128.7, 127.1, 125.8, 125.8, 123.8, 122.5, 117.4, 109.5, 44.0, 39.6, 36.8. HRMS (ESI): *m/z* calcd for $C_{19}H_{15}F_3N_4O_2S$ 421.0941 found 421.0938 $[M+H]^+$.

*2.4.2.19. (2E,5Z)-2-((4-chlorobenzyl)imino)-5-(8-oxo-5,6,7,8-tetrahydropyrrolo [2,3-c] azepin-4(1H)-ylidene)thiazolidin-4-one (**12d**).* Pale yellow; 86% yield; mp: 235–237 °C; FT-IR (cm^{-1}): 3256, 3215, 3065, 2911, 1698, 1661, 1637, 1589, 1517, 1473, 1387, 1345, 1148, 745, 697, 485; ^{1}H NMR (500 MHz, DMSO-d_6): δ 12.12 (s, 1H), 9.35 (s, 1H), 8.04 (t, $J = 5.2$ Hz, 1H), 7.39 (d, $J = 8.5$ Hz, 2H), 7.32 (d, $J = 8.5$ Hz, 2H), 7.08 (t, $J = 2.9$ Hz, 1H), 6.50 (t, $J = 2.6$ Hz, 1H), 4.86 (s, 2H), 3.48–3.46 (m, 2H), 3.26–3.23 (m, 2H). ^{13}C NMR (125 MHz, DMSO-d_6): δ 165.8, 163.9, 153.7, 142.0, 136.2, 132.3, 130.0, 128.9, 127.0, 123.8, 122.4, 117.4, 109.6, 60.2, 43.7, 36.8. HRMS (ESI): *m/z* calcd for $C_{18}H_{15}ClN_4O_2S$ 387.0677 found 387.0674 $[M+H]^+$ and 389.1106 $[M+2]^+$.

*2.4.2.20. (2E,5Z)-2-((3-chlorobenzyl)imino)-5-(8-oxo-5,6,7,8-tetrahydropyrrolo [2,3-c] azepin-4(1H)-ylidene)thiazolidin-4-one (**12e**).* Pale yellow; 81% yield; mp: 217–219 °C; FT-IR (cm^{-1}): 3174, 3058, 2942, 1695, 1644, 1469, 1613, 1562, 1422, 1377, 1336, 1268, 1141, 1080, 936, 779, 742, 697, 680, 608, 537, 489; ^{1}H NMR (500 MHz, DMSO-d_6): δ 12.10 (s, 1H), 9.35 (s, 1H), 8.02 (t, $J = 5.1$ Hz, 1H), 7.37–7.36 (m, 1H), 7.35–7.34 (m, 1H), 7.27–7.25 (m, 1H), 7.08 (t, $J = 2.9$ Hz, 1H), 6.51 (t, $J = 2.6$ Hz, 1H), 4.88 (s, 2H), 3.49–3.47 (m, 2H), 3.25 (dd, $J = 11.0$, 5.2 Hz, 2H). ^{13}C NMR (125 MHz, DMSO-d_6): δ 165.8, 163.9, 153.7, 142.2, 139.7, 133.4, 130.8, 128.0, 127.8, 127.1, 126.8, 123.8, 122.5, 117.4,

109.6, 43.8, 41.6, 36.8. HRMS (ESI): *m/z* calcd for $C_{18}H_{15}ClN_4O_2S$ 387.0677 found 387.0678 $[M+H]^+$ and 389.0647 $[M+2]^+$.

2.4.2.21. (2E,5Z)-2-((2-chlorobenzyl)imino)-5-(8-oxo-5,6,7,8-tetrahydropyrrolo [2,3-c] azepin-4(1H)-ylidene)thiazolidin-4-one ***(12f)***. Beige; 81% yield; mp: 214–216 °C; FT-IR (cm^{-1}): 3 243, 3147, 3038, 2884, 1695, 1630, 1586, 1534, 1480, 1446, 1415, 1387, 1353, 1159, 1107, 1090, 1042, 960, 755, 735, 608, 547; ^{1}H NMR (500 MHz, DMSO-d_6): δ 12.14 (s, 1H), 9.34 (s, 1H), 8.05 (t, $J = 5.2$ Hz, 1H), 7.48 (dd, $J = 5.8$, 3.4 Hz, 1H), 7.30 (dd, $J = 6.1$, 3.2 Hz, 2H), 7.10 (t, $J = 2.9$ Hz, 1H), 7.00 (dd, $J = 5.6$, 3.8 Hz, 1H), 6.54 (t, $J = 2.7$ Hz, 1H), 4.94 (s, 2H), 3.47 (dd, $J = 6.6$, 4.4 Hz, 2H), 3.26 (dd, $J = 11.2$, 5.1 Hz, 2H). ^{13}C NMR (125 MHz, DMSO-d_6): δ 170.5, 168.6, 158.3, 147.0, 138.7, 136.7, 134.6, 133.9, 132.6, 132.2, 131.9, 128.3, 127.3, 122.2, 114.4, 114.3, 47.0, 44.4, 41.6. HRMS (ESI): *m/z* calcd for $C_{18}H_{16}ClN_4O_2S$ 387.0677 found 387.0693 $[M+H]^+$ and 389.0652 $[M+2]^+$.

2.4.2.22. (2E,5Z)-2-((4-methylbenzyl)imino)-5-(8-oxo-5,6,7,8-tetrahydropyrrolo [2,3-c] azepin-4(1H)-ylidene)thiazolidin-4-one ***(12g)***. Brownish; 92% yield; mp: 243–245 °C; FT-IR (cm^{-1}): 3270, 3202, 3058, 2918, 1695, 1651, 1616, 1572, 1517, 1466, 1428, 1384, 1357, 1340, 1309, 1264, 1152, 1094, 930, 783, 759, 738, 625, 489, 472; ^{1}H NMR (500 MHz, DMSO-d_6): δ 12.10 (s, 1H), 9.31 (s, 1H), 8.02 (t, $J = 5.2$ Hz, 1H), 7.20 (d, $J = 8.1$ Hz, 2H), 7.12 (d, $J = 8.2$ Hz, 2H), 7.07 (t, $J = 2.9$ Hz, 2H), 6.50 (t, $J = 2.6$ Hz, 1H), 4.83 (s, 2H), 3.48–3.46 (m, 2H), 3.24 (dd, $J = 10.9$, 5.2 Hz, 2H), 2.27 (s, 3H). ^{13}C NMR (125 MHz, DMSO-d_6): δ 165.8, 163.9, 153.7, 141.8, 136.9, 134.2, 129.4, 128.2, 127.0, 123.8, 122.4, 117.6, 109.5, 44.1, 39.5, 36.7, 21.2. HRMS (ESI): *m/z* calcd for $C_{19}H_{18}N_4O_2S$ 367.1223 found 367.1222 $[M+H]^+$.

2.4.2.23. (2E,5Z)-2-((4-(tert-butyl)benzyl)imino)-5-(8-oxo-5,6,7,8-tetrahydropyrrolo [2,3-c]azepin-4(1H)-ylidene)thiazolidin-4-one ***(12h)***. Pale orange; 93% yield; mp: 267–269 °C; FT-IR (cm^{-1}): 3219, 3055, 2966, 2867, 1072, 1623, 1586, 1534, 1480, 1425, 1387, 1346, 1264, 1107, 936, 882, 779, 742, 595, 564; ^{1}H NMR (500 MHz, DMSO-d_6): δ 12.08 (s, 1H), 9.31 (s, 1H), 8.01 (t, $J = 5.1$ Hz, 1H), 7.34 (d, $J = 8.4$ Hz, 2H), 7.24 (d, $J = 8.4$ Hz, 2H), 7.07 (t, $J = 2.9$ Hz, 1H), 6.50 (t, $J = 2.6$ Hz, 1H), 4.84 (s, 2H), 3.49–3.47 (m, 2H), 3.25 (dd, $J = 11.0$, 5.2 Hz, 2H), 1.26 (s, 9H). ^{13}C NMR (125 MHz, DMSO-d_6): δ 165.8, 163.9, 153.7, 150.1, 141.8, 134.2, 127.9, 127.0, 125.6, 123.8, 122.4, 117.6, 109.5, 44.0, 39.5, 36.7, 34.7, 31.6. HRMS (ESI): *m/z* calcd for $C_{22}H_{24}N_4O_2S$ 409.1693 found 409.1691 $[M+H]^+$.

2.4.2.24. (2E,5Z)-2-((4-fluorobenzyl)imino)-5-(8-oxo-5,6,7,8-tetrahydropyrrolo [2,3-c] azepin-4(1H)-ylidene)thiazolidin-4-one ***(12i)***. Pale yellow; 80% yield; mp: 280–282 °C; FT-IR (cm^{-1}): 3294, 3198, 3079, 2956, 1692, 1647, 1616, 1558, 1528, 1510, 1469, 1425, 1384, 1336, 1271, 1223, 1141, 1097, 930, 841, 769, 728, 619, 581, 485; ^{1}H NMR (500 MHz, DMSO-d_6): δ 12.11 (s, 1H), 9.35 (s, 1H), 8.04 (t, $J = 5.0$ Hz, 1H), 7.38–7.35 (m, 2H), 7.17–7.14 (m, $J = 7.2$ Hz, 2H), 7.08 (t, $J = 2.9$ Hz, 1H), 6.50 (t, $J = 2.6$ Hz, 1H), 4.86 (s, 2H), 3.49–3.46 (m, 2H), 3.25 (dd, $J = 10.8$, 5.2 Hz, 2H). ^{13}C NMR (125 MHz, DMSO-d_6): δ 165.8, 163.9, 161.8 (d, $J_{CF} = 243.0$ Hz), 153.7, 142.0, 133.4 (d, $J_{CF} = 3.0$ Hz), 130.3 (d, $J_{CF} = 8.2$ Hz), 127.0, 123.8, 122.5, 117.5, 115.6 (d, $J_{CF} = 21.4$ Hz), 109.5, 43.6, 39.5, 36.7. HRMS (ESI): *m/z* calcd for $C_{18}H_{15}FN_4O_2S$ 371.0373 found 371.0978 $[M+H]^+$.

2.4.2.25. (2E,5Z)-2-((benzo[d] [1,3]dioxol-5-ylmethyl)imino)-5-(8-oxo-5,6,7,8-tetra hydropyrrolo [2,3-c]azepin-4(1H)-ylidene)thiazolidin-4-one ***(12j)***. Brownish orange; 86% yield; mp: 227–229 °C; FT-IR (cm^{-1}): 3291, 3205, 3072, 2959, 2905, 1688, 1651, 1620, 1531, 1504, 1473, 1425, 1384, 1329, 1261, 1138, 1100, 1042, 936, 889, 772, 731, 646, 530, 499; ^{1}H NMR (500 MHz, DMSO-d_6): δ 12.10 (s, 1H), 9.33 (s, 1H), 8.03 (t, $J = 5.2$ Hz, 1H), 7.07 (t, $J = 2.9$ Hz, 1H), 6.90 (d, $J = 1.5$ Hz, 1H), 6.85 (d, $J = 7.9$ Hz, 1H), 6.81 (dd, $J = 8.0$, 1.6 Hz, 1H), 6.50 (t, $J = 2.6$ Hz, 1H), 5.99 (s, 2H), 4.77 (s, 2H), 3.48 (dd, $J = 7.0$, 4.1 Hz, 2H), 3.25 (dd, $J = 11.1$, 5.0 Hz, 2H). ^{13}C NMR (125 MHz, DMSO-d_6): δ 165.7, 163.9, 147.6, 147.0, 142.0, 140.9, 130.9, 127.0, 123.8, 122.5, 121.8, 117.5, 109.5, 109.0, 108.6, 101.4, 44.1, 39.4, 36.7. HRMS (ESI): *m/z* calcd for $C_{19}H_{16}N_4O_2S$ 397.0965 found 397.0963 $[M+H]^+$.

2.4.2.26. (2E,5Z)-2-((4-methoxybenzyl)imino)-5-(1-methyl-8-oxo-5,6,7,8-tetrahydro pyrrolo [2,3-c]azepin-4(1H)-ylidene)thiazolidin-4-one ***(12k)***. Beige; 90% yield; mp: 249–251 °C; FT-IR (cm^{-1}): 3325, 3192, 3051, 2918, 1695, 1661, 1623, 1562, 1517, 1490, 1469, 1425, 137, 1333, 1521, 1128, 107, 1090, 1015, 930, 779, 725, 738; ^{1}H NMR (500 MHz, DMSO-d_6): δ 9.31 (s, 1H), 8.09 (t, $J = 5.9$ Hz, 1H), 7.39 (d, $J = 8.5$ Hz, 2H), 7.32 (d, $J = 8.5$ Hz, 2H), 7.12 (d, $J = 2.8$ Hz, 1H), 6.37 (d, $J = 2.8$ Hz, 1H), 4.85 (s, 2H), 3.80 (s, 3H), 3.33 (s, 3H), 3.32 (dd, $J = 6.7$, 4.3 Hz, 2H), 3.22 (dd, $J = 11.1$, 5.6 Hz, 2H). ^{13}C NMR (125 MHz, DMSO-d_6): δ 165.4, 164.3, 153.9, 141.9, 136.2, 132.3, 130.0, 128.8, 127.8, 126.0, 124.5, 119.1, 107.7, 43.6, 39.4, 38.8, 36.3. HRMS (ESI): *m/z* calcd for $C_{20}H_{20}N_4O_3S$ 397.0965 found 397.0963 $[M+H]^+$.

2.4.2.27. (2E,5Z)-5-(8-oxo-5,6,7,8-tetrahydropyrrolo [2,3-c]azepin-4(1H)-ylidene)-2-(phenethylimino)thiazolidin-4-one ***(12l)***. Brownish orange; 90% yield; mp: 257–259 °C; FT-IR (cm^{-1}): 3267, 3209, 3028, 2952, 1644, 1678, 1603, 1480, 1428, 1411, 1353, 1346, 1264, 1145, 1128, 994, 936, 868, 776, 745, 697, 608, 492; ^{1}H NMR (500 MHz, DMSO-d_6): δ 12.08 (s, 1H), 9.28 (s, 1H), 8.01 (t, $J = 5.1$ Hz, 1H), 7.32–7.29 (m, 2H), 7.22–7.21 (m, 3H), 7.07 (t, $J = 2.8$ Hz, 1H), 6.48 (t, $J = 2.6$ Hz, 1H), 3.91–3.88 (m, 2H), 3.45–3.43 (m, 2H), 3.23 (dd, $J = 11.0$, 5.2 Hz, 2H), 2.87 (dd, $J = 8.6$, 6.8 Hz, 2H). ^{13}C NMR (125 MHz, DMSO-d_6): δ 165.8, 163.9, 153.7, 141.8, 136.9, 134.2, 129.4, 128.2, 127.0, 123.8, 122.4, 117.6, 109.5, 44.0, 40.6, 36.7, 21.1. HRMS (ESI): *m/z* calcd for $C_{19}H_{218}N_4O_2S$ 367.1223 found 367.1224 $[M+H]^+$.

2.4.2.28. (2E,5Z)-2-((4-methoxyphenethyl)imino)-5-(8-oxo-5,6,7,8-tetrahydropyrrolo [2,3-c]azepin-4(1H)-ylidene)thiazolidin-4-one ***(12m)***. Brownish orange; 89% yield; mp: 245–247 °C; FT-IR (cm^{-1}): 3397, 3277, 3192, 2956, 2932, 1678, 1634, 1613, 1579, 1531, 1510, 1490, 1425, 1394, 1350, 1148, 1131, 1107, 1029, 885, 783, 752, 646; ^{1}H NMR (500 MHz, DMSO-d_6): δ 12.07 (s, 1H), 9.26 (s, 1H), 8.01 (t, $J = 5.1$ Hz, 1H), 7.12 (d, $J = 8.5$ Hz, 2H), 7.07 (t, $J = 2.9$ Hz, 1H), 6.86 (d, $J = 8.5$ Hz, 2H), 6.48 (t, $J = 2.6$ Hz, 1H), 3.87–3.84 (m, 2H), 3.72 (S, 3H), 3.45 (dd, $J = 7.2$, 3.9 Hz, 2H), 3.24 (dd, $J = 10.9$, 5.2 Hz, 2H), 2.80 (dd, $J = 8.6$, 6.8 Hz, 2H). ^{13}C NMR (125 MHz, DMSO-d_6): δ 165.7, 163.8, 158.3, 153.6, 141.3, 130.7, 130.1, 126.9, 123.9, 122.4, 117.7, 114.3, 109.5, 55.5, 42.7, 39.7, 36.3, 32.2. HRMS (ESI): *m/z* calcd for $C_{19}H_{218}N_4O_2S$ 397.1329 found 397.1324 $[M+H]^+$.

2.4.3. Biological assay methods

2.4.3.1. Cell culture. Cells were obtained from National Centre for Cell Sciences (NCCS), Pune, India and stocks were maintained in the laboratory. A549 - lung cancer cells, HCT-116 - human colon cancer, SK-MEL-28 - human melanoma cell line, HT-29 – caucasian colon adenocarcinoma, MCF-7 - breast adenocarcinoma, NRK – normal rat kidney epithelial cells were grown in tissue culture flasks in DMEM (Dulbecco Modified Eagle Medium), Sigma or RPMI (Roswell Park Memorial Institute medium) supplemented with 10% fetal bovine serum with 1X stabilized antibiotic-antimycotic solution (Sigma) in a CO_2 incubator at 37 °C with 5% CO_2 and 90% relative humidity.

2.4.3.2. Evaluation of cytotoxicity with MTT assay. The cytotoxicity of these heteroarylazepinones-thiazolidinones conjugates was determined using an MTT assay. Cell lines (A549, HCT-116, SK-MEL-28, HT-29, MCF-7 and NRK) were used in this assay. 1X104 cells/well were seeded in 200 μL Dulbecco's modified Eagle's medium (DMEM) supplemented with 10% FBS in each well of 96-well microculture plates and

incubated for 24 h at 37 °C in a CO_2 incubator. All the derivatives diluted to the desired concentrations (500 *n*M, 1 μM, 5 μM, 10 μM, 25 μM, 50 μM, 75 μM, 100 μM and 150 μM) in culture medium, were added to the wells with respective vehicle as control. 5-Fluorouracil- and doxorubicin-treated cells, in the same concentration range, were used as standards. After 48 h of incubation period, 10 μL MTT (3-(4,5-dimethylthiazol-2-yl)-2,5-diphenyltetrazoliumbromide) (5 mg/mL) was added to each well and the plates were incubated for 4 h. The supernatant was then carefully removed from each well plate and the formed formazan crystals were dissolved in 100 μL of DMSO and the absorbance at 570 nm wavelength was recorded using an ELx800 microplate reader (BioTek, USA). The assay was repeated thrice and means values were considered.

2.4.4. Apoptosis detection and growth inhibition studies

2.4.4.1. Morphological observations. A549 and SK-MEL-28 cells were seeded at a density of 1x105 cells/mL in 6 well plates and were treated with compounds **11g** and **12g**, respectively, at various concentrations (**11g**: 0.625, 1.25 and 2.5 μM and **12g**: 2.08, 4.16 and 8.32 μM). After 48 h of treatment, morphological changes in the cells were observed and images were captured under a phase-contrast microscope (Nikon, Inc. Japan).

2.4.4.2. Acridine orange/ethidium bromide (AO/EB) staining. A549 and SK-MEL-28 cells were plated at a concentration of 1x106 cells/mL were treated with compounds **11g** and **12g** at concentrations of 0.625, 1.25 and 2.5 μM and 2.08, 4.16 and 8.32 μM, respectively. Plates were incubated for 48 h at 37 °C 10 μL each from 1 mg/mL stock solution of fluorescent dyes containing acridine orange (AO) ethidium bromide (EB) were added into each well in equal volumes (10 μg/mL), respectively. Cells were visualized under a fluorescence microscope (Nikon, Inc. Japan) with excitation (488 nM) and emission (550 nM) at 200X magnification.

2.4.4.3. DAPI nucleic acid staining. Nuclear morphological changes were observed by DAPI staining. After treatment with compounds **11g** and **12g** (0.625, 1.25 and 2.5 μM and 2.08, 4.16 and 8.32 μM, respectively) for 48 h, A549 and SK-MEL-28 cells were washed with PBS and permeabilized with 0.1% Tween 20 for 10 min followed by staining with DAPI. Control and compound- and camptothecin-treated cells were observed with a fluorescence microscope with excitation at 359 nM and emission at 461 nM using a DAPI filter at 200X magnification.

2.4.4.4. Reactive oxidative species (ROS) generation. The A549 and SK-MEL-28 cells were plated at 1 × 105 cells/mL in 24-well culture plates and allowed to adhere overnight. Cells were treated with camptothecin, compounds **11g** and **12g** for 48 h, washed with PBS and fixed with 4% paraformaldehyde. Cells were exposed with Carboxy-DCFDA dye (life technologies) (10 μM) for 30 min in the dark at room temperature and washed with PBS to remove the excess dye. The increase in the intensity of fluorescence because of the generation of reactive oxygen species was analyzed using a fluorescence microscope (Nikon).

2.4.4.5. In vitro cell migration assay/wound-healing assay. A549 and SK-MEL-28 cells were plated at a cell density of 3.5 × 105 cells/well into 12-well plates in RPMI medium and allowed to form a confluent monolayer, and then the scratch is made with 200 μL sterile pipette tip and then treated with 0.625, 1.25 and 2.5 μM and 2.08, 4.16 and 8.32 μM of the compounds **11g** and **12g**, respectively. The migration of lung cancer cells was captured by microscopic observations at 0 h and 48 h.

2.4.4.6. Clonogenic growth inhibition assay. A549 and SK-MEL-28 cells in the exponential growth phase were seeded into 6-well plates at 4000 cells/well. After 24 h incubation, the culture medium was replaced with a medium containing increasing concentration (0.625, 1.25 and 2.5 μM and 2.08, 4.16 and 8.32 μM) of compounds **11g** and **12g**, respectively and 1% DMSO (control). The cells were incubated for 7 days and the drug-containing medium was replenished after 3 days. Each treatment was performed in triplicate. After incubation, the cells were washed twice with PBS, fixed with 4% paraformaldehyde for 20 min and stained with crystal violet for a further 15 min.

2.4.4.7. Annexin V-FITC/PI staining assay. A549 and SK-MEL-28 cells (1x106 cells/mL) were seeded in six-well plates and allowed to grow overnight. The medium was then replaced with complete medium containing compounds **11g** and **12g** at 0.625, 1.25 and 2.5 μM and 2.08, 4.16 and 8.32 μM concentrations, respectively. After 48 h of treatment, cells from the supernatant and adherent monolayer cells were harvested by trypsinization, washed with PBS at 3000 rpm. Then the cells were processed with Annexin V-assay kit (FITC Annexin V Apoptosis Detection Kit, BD Pharmingen™) according to the instructions given by the manufacturer. Further, flow cytometric analysis was performed using a flow cytometer (BD FACSVerse™, USA) and compared with camptothecin.

2.4.5. DNA binding studies

2.4.5.1. UV–Visible studies. UV–Visible spectroscopy titrations were performed using ABI Lambda 40 UV–Vis spectrophotometer (Foster City, USA) at 25 °C using a 1 cm path length quartz cuvette. Stock solutions of 1 mM of CT-DNA (calf thymus DNA, which can form perfect double-stranded DNA structure) were prepared in 100 mM *Tris*-HCl (pH 7.0). 1 mM stock solutions of the synthesized compounds **11g** and **12g** were prepared by dissolving them in 1:1 DMSO: Milli Q water. UV–Visible absorption titrations are performed by adding 10 μM CT-DNA solution in 100 mM *Tris*-HCl (pH 7.0) each time to the quartz cuvette containing about 10 μM of compounds **11g** and **12g** solutions. Since **11g** molecule has an absorbance at 260 nm, (matching with DNA absorption), in order to remove the error in absorption titration assay, each time same concentration of CT-DNA was added to reference cuvette also along with sample cuvette containing **11g** sample. Titrations were carried out until the complex absorption band remained at a fixed wavelength upon five successive additions of CT-DNA. UV–Vis spectra were recorded from 200 to 500 nm range.

2.4.5.2. Circular dichroism spectroscopy. Circular dichroism experiments were carried out using JASCO 815 CD spectropolarimeter (Jasco, Tokyo, Japan). CD spectrum was recorded from 220 to 320 nm to find the conformational changes in CT-DNA after DNA-compound interaction. For CD experiments, 10×10^{-6} M of CT-DNA was used. For characterizing compound-CT-DNA interaction, CD spectra were recorded in 1:0, 1:1 and 1:2 M ratios of CT-DNA:compound **11g**/**12g**. CD titrations were performed in 100 mM *Tris*-HCl (pH 7.0) at 25 °C. Each CD spectrum was recorded thrice and the average of three scans was considered.

2.4.5.3. Relative viscosity studies. Viscosity experiments were conducted using Ostwald viscometer immersed in a water bath and maintained at 25 °C. Viscosity experiments were performed for compounds **11g** and **18g** (15 μM), after mixing them with CT-DNA solution (150 μM). Before mixing CT-DNA and compound **11g**/**12g**, viscosity measurements were performed with CT-DNA alone. EtBr and Hoechst 33342 complex with CT-DNA were considered as control. DNA solution was prepared in 100 mM *Tris*-HCl (pH 7.0). A graph was drawn by plotting $(\eta/\eta_o)^{1/3}$ versus compound/CT-DNA, where η is the viscosity of CT-DNA in the presence of compound **11g**/**12g** and η_o is the viscosity of CT-DNA alone. Viscosity values were calculated according to the protocol mentioned by Tan *et al.* [74].

2.4.6. Topoisomerase I and II inhibition studies

2.4.6.1. Topoisomerase I inhibition assay. Topoisomerase I inhibitory activity was measured using a DNA cleavage assay as described previously [75]. pBR322 plasmid DNA was purchased from Sigma Aldrich, USA and 0.5 μg of pBR322 DNA was incubated with 1 unit of Topo I enzyme (Invitrogen) in 1X NEB buffer (50 mM potassium acetate, 20 mM Tris acetate, 10 mM magnesium acetate, 1 mM DTT). The synthetic derivatives (compounds **11g** and **12g)** at 10 μM (final concentration) were separately added to the Topo I-DNA complex and incubated at 37 °C for 30 min, allowing the formation of the ternary enzyme-DNA-ligand complex. 10 μM camptothecin (final concentration) was used as a control. Then the enzyme was inactivated by thermal denaturation at 65 °C. After the incubation, the samples were resolved using 1% agarose gel electrophoresis which enabled the visualization of cleavage products. The pBR 322 DNA sample to which no ligand was added acted as a positive control.

2.4.6.2. Topoisomerase I relaxation assay for determination of IC_{50} values. Supercoiled pHOT1 DNA (0.5 mg) was incubated with 4 units of human topoisomerase I in relaxation buffer (10 mM Tris-HCl (pH 7.8), 1 mM EDTA, 0.15 M NaCl, 0.1% BSA, 0.1 spermidine, 5% glycerol), in the presence of varying concentrations (20, 40, 60 and 80 μM) of the **11g** and **12g.** The assay was carried out under the similar conditions with 20 μM camptothecin (CPT) (a positive control). 20 μM camptothecin (CPT) was considered in the assay as it was reported earlier [74] that at 20 μM is the IC_{50} for Camptothecin (CPT). Topo I inhibition assay was carried out at 37 °C for 1 h and then reaction was terminated by the addition of 0.25% of sodium dodecyl sulfate (SDS) and 50 mg/mL proteinase K to. The reaction mixture was subjected to electrophoresis through a 1% agarose gel. After the gel run, the agarose gel was stained with 0.5 mg/mL ethidium bromide in TAE buffer (40 mM Tris-borate and 1 mM EDTA). After staining the gel with ethidium bromide, it is photographed under UV light. For the quantitative determination of topoisomerase activity as different **11g** and **12g** concentration, photographic negatives were scanned and the area representing supercoiled DNA, migrating as a single band at the bottom of the gel was measured using Syngene G Box gel documentation and analysis system (SyngenBiotech, Sacramento, CA). The concentrations of the inhibitor that prevented 50% of the supercoiled DNA from being converted into relaxed DNA (IC_{50} values) were determined by averaging the data from three different assays. This assay at varying concentration of **11g** and **12g** was carried out as reported earlier [76]. The IC_{50} values were calculated following the procedure mention by Arvind Negi *et al.* [77].

2.4.6.3. Topoisomerase II inhibition assay. In order to test the role of synthetic **11g** and **12g** in Topo II inhibition, decatenation of kDNA was carried out using the protocol mentioned in the Topo II Drug Screening Kit (TG 1009, Topogen, USA). Topoisomerase II inhibition was assayed using the ATP-dependent decatenation of kDNA. Reactions were carried out in 20 μL and contained 120 mM KCl, 50 mM Tris-HCl, pH 8, 10 mM $MgCl_2$, 0.5 mM dithiothreitol, 0.5 mM ATP, 30 mg/mL bovine serum albumin, 200–300 ng of kDNA, and topoisomerase II. The amount of topoisomerase II (5 units) was adjusted in preliminary experiments to decatenate approximately 100% of the kDNA under our assay conditions. Authentic decatenated DNA was used as the controls to identify decatenated kDNA. The reactions in the presence and absence of **11g** and **12g** were incubated at 37 °C for 30 min and the reaction was terminated by the addition of 2 μL of a stop buffer containing 10% (w/v) SDS and 2 μl of 0.5 mg/mL proteinase K and incubated for 10 min at 37 °C. After the completion of the reaction, the products in the reaction mixture were separated by 1% agarose gel. The products in the agarose gel were visualized after staining with ethidium bromide (0.5 μg mL-1). The gels were run at 100 V for about 40 min and visualized under UV transillumination (BIO-RAD gel doc XR+, USA).

2.4.7. Molecular modeling studies

2.4.7.1. Docking simulation study. Molecular docking studies were performed by using Maestro, version 11.1 of Schrödinger suite 2017–1 [69]. The protein structure of human DNA topoisomerase I (70 kDa) in complex with the poison topotecan along with covalent complex with a 22 base pair DNA duplex (PDB code: 1K4T, resolution 2.1 Å) was obtained from the RCSB PDB. It was prepared using the Protein Preparation Wizard, wherein the protein was hydrogenated and those protons which are necessary to define the correct ionization and tautomerization of protein were also included at pH 7.0. The missing or incomplete residues were repaired by employing the Prime module. OPLS-2005 force field was used to attenuate steric clashes that may exist in the structures under study. The energy minimization was done until the energy was found to converge or the Root Mean Square Deviation (RMSD) reached a maximum cut-off of 0.30 Å. Water molecules beyond 5 Å from hetero groups were deleted.

Molecular docking was done keeping the grid box of size 12 Å from the centroid to ensure complete coverage of the active site. To start with, the active site was defined by using the co-crystals of the respective proteins, followed by the validation of docking protocol which was achieved by re-docking the bound-ligand at the active site of human DNA topoisomerase I. Following this, the investigated compounds were docked at the active sites of human DNA topoisomerase I and the results were compared with the co-crystallized ligand.

2.4.7.2. In silico physico-chemical and ADME/T studies. Physico-chemical and ADME/T properties, which help in predicting both physico-chemical significant descriptors and pharmacokinetically important properties of the molecules, were calculated using the Qikprop module of Schrödinger suite 2017–1 [71]. QikProp enumerates the comparative ranges of a molecule's properties with those of known drugs. Major parameters of the designed molecules that enabled us to quickly evaluate the physico-chemical and ADME/T properties of the designed 4-thiazolidinone conjugates of indolo- and pyrroloazepinone are discussed.

Declaration of competing interest

The authors declare that they have no known competing financial interests or personal relationships that could have appeared to influence the work reported in this paper.

Appendix A. Supplementary data

Supplementary data to this article can be found online at https://doi.org/10.1016/j.ejmech.2022.114465.

References

[1] N. Shankaraiah, S. Nekkanti, O. Ommi, P.S.L. Soukya, Diverse targeted approaches to battle multidrug resistance in cancer, Curr. Med. Chem. 26 (39) (2019) 7059–7080.
[2] N.P. Kumar, P. Sharma, T.S. Reddy, S. Nekkanti, N. Shankaraiah, G. Lalita, S. Sujanakumari, S.K. Bhargava, V.G.M. Naidu, A. Kamal, Synthesis of 2,3,6,7-Tetramethoxyphenanthren-9-amine: an efficient precursor to access new 4-Aza-2,3-dihydropyridophenanthrenes as apoptosis inducing agents, Eur. J. Med. Chem. 127 (2017) 305–317.
[3] A. Kamal, K. Sreekanth, P.P. Kumar, N. Shankaraiah, G. Balakishan, M.J. Ramaiah, S.N.C.V.L. Pushpavalli, P. Ray, M.P. Bhadra, Synthesis and potential cytotoxic activity of new phenanthrylphenol-pyrrolobenzodiazepines, Eur. J. Med. Chem. 45 (2010) 2173–2181.
[4] R. Tokala, S. Thatikonda, S. Sana, C. Godugu, N. Shankaraiah, Synthesis and *In vitro* cytotoxicity evaluation of β-carboline-linked 2,4-thiazolidinedione hybrids: potential DNA intercalation and apoptosis inducing studies, New J. Chem. 42 (2018) 16226–16236.
[5] A. Kamal, P. Suresh, M.J.P. Ramaiah, T.S. Reddy, R.K. Kapavarapu, S. Imthiajali, T. L.N. Reddy, S.N.C.V.L. Pushpavalli, N. Shankaraiah, M.-P. Bhadra, 4β-[4'-(1-(Aryl) ureido)benzamide]podophyllotoxins as DNA topoisomerase I and IIα inhibitors and apoptosis inducing agents, Bioorg. Med. Chem. 21 (2013) 5198–5208.

[6] N.S. Rao, N. Nagesh, V.L. Nayak, S. Sunkari, R. Tokala, N. Shankaraiah, A. Kamal, Design and synthesis of DNA-intercalative naphthalimide-benzothiazole/cinnamide derivatives: cytotoxicity evaluation and topoisomerase IIα inhibition, MedChemComm 10 (2019) 72–79.
[7] M. Sathish, S.C. Dushantrao, S. Nekkanti, R. Tokala, S. Thatikonda, Y. Tangella, G. Srinivas, S. Cherukommu, N.H. Krishna, N. Shankaraiah, N. Nagesh, A. Kamal, Synthesis of DNA interactive C3-Trans-cinnamide linked β-carboline conjugates as potential cytotoxic and DNA topoisomerase I inhibitors, Bioorg. Med. Chem. 26 (2018) 4916–4929.
[8] L.H. Hurley, DNA and its associated processes as targets for cancer therapy, Nat. Rev. Cancer 2 (3) (2002) 188–200.
[9] R. Martinez, L. Chacon-Garcia, The search of DNA-intercalators as antitumoral drugs: what it worked and what did not work, Curr. Med. Chem. 12 (2) (2005) 127–151.
[10] a) M. Kadagathur, G.P. Devi, P. Grewal, D.K. Sigalapalli, P.N. Makhal, U. C. Banerjee, N.B. Bathini, N.D. Tangellamudi, Novel diindoloazepinone derivatives as DNA minor groove binding agents with selective topoisomerase I inhibition: design, synthesis, biological evaluation and docking studies, Bioorg. Chem. 99 (2020) 103629;
b) M. Kadagathur, A.S. Shaikh, B. Panda, J. George, R. Phanindranath, D. K. Sigalapalli, N.A. Bhale, C. Godugu, N. Nagesh, N. Shankaraiah, N. D. Tangellamudi, Synthesis of indolo/pyrroloazepinone-oxindoles as potential cytotoxic, DNA-intercalating and Topo I inhibitors, Bioorg. Chem. 25 (122) (2022), 105706.
[11] a) X. Cai, P.J. Gray, D.D. Von Hoff, DNA minor groove binders: back in the groove, Cancer Treat Rev. 35 (5) (2009) 437–450;
b) S. Nekkanti, R. Tokala, N. Shankaraiah, Targeting DNA minor groove by hybrid molecules as anticancer agents, Curr. Med. Chem. 24 (26) (2017) 2887–2907.
[12] M. Szyf, The DNA methylation machinery as a target for anticancer therapy, Pharmacol. Ther. 70 (1) (1996) 1–37.
[13] D.A. Burden, N. Osheroff, Mechanism of action of eukaryotic topoisomerase II and drugs targeted to the enzyme, Biochim. Biophys. Acta Gene Struct. Expr. 1400 (1–3) (1998) 83–106.
[14] C. Kunick, Z. Zeng, R. Gussio, D. Zaharevitz, M. Leost, F. Totzke, C. Schächtele, M. H.G. Kubbutat, L. Meijer, T. Lemcke, Structure-aided of optimization of kinase inhibitors derived from alsterpaullone, ChemBioChem 6 (3) (2005) 541–549.
[15] C. Schultz, A. Link, M. Leost, D.W. Zaharevitz, R. Gussio, E.A. Sausville, L. Meijer, C. Kunick, Paullones, a series of cyclin-dependent kinase inhibitors: synthesis, evaluation of CDK1/cyclin B inhibition, and *in vitro* antitumor activity, J. Med. Chem. 42 (15) (1999) 2909–2919.
[16] D.W. Zaharevitz, R. Gussio, M. Leost, A.M. Senderowicz, T. Lahusen, C. Kunick, L. Meijer, E.A. Sausville, Discovery and initial characterization of the paullones, a novel class of smallmolecule inhibitors of cyclin-dependent kinases, Cancer Res. 59 (11) (1999) 2566–2569.
[17] V. Sharma, J.J. Tepe, Potent inhibition of checkpoint kinase activity by a hymenialdisine-derived indoloazepine, Bioorg. Med. Chem. Lett. 14 (16) (2004) 4319–4321.
[18] M. Knockaert, K. Wieking, S. Schmitt, M. Leost, K.M. Grant, J.C. Mottram, C. Kunick, L. Meijer, Intracellular targets of paullones: identification following affinity purification on immobilized inhibitor, J. Biol. Chem. 277 (2002) 25493–25501.
[19] Y. Wan, W. Hur, C.Y. Cho, Y. Liu, F.J. Adrian, O. Lozach, S. Bach, T. Mayer, D. Fabbro, L. Meijer, N.S. Gray, Synthesis and target identification of hymenialdisine analogs, Chem. Biol. 11 (2004) 247–259.
[20] J. Xie, J. Tian, L. Su, M. Huang, X. Zhu, F. Ye, Y. Wan, Pyrrolo[2,3-c]Azepine derivatives: a new class of potent protein tyrosine phosphatase 1B inhibitors, Bioorg. Med. Chem. Lett. 21 (14) (2011) 4306–4309.
[21] D. Tasdemir, R. Mallon, M. Greenstein, L.R. Feldberg, S.C. Kim, K. Collins, D. Wojciechowicz, G.C. Mangalindan, G.P. Concepcion, M.K. Harper, C.M. Ireland, Aldisine alkaloids from the philippine sponge stylissa massa are potent inhibitors of mitogen-activated protein kinase kinase-1 (MEK-1), J. Med. Chem. 45 (2002) 529–532.
[22] A. Putey, F. Popowycz, Q.T. Do, P. Bernard, S.K. Talapatra, F. Kozielski, C. M. Galmarini, B. Joseph, Indolobenzazepin-7-Ones and 6-, 8-, and 9-membered ring derivatives as tubulin polymerization inhibitors: synthesis and structure-activity relationship studies, J. Med. Chem. 52 (19) (2009) 5916–5925.
[23] Y. Drew, E.A. Mulligan, W.T. Vong, H.D. Thomas, S. Kahn, S. Kyle, A. Mukhopadhyay, G. Los, Z. Hostomsky, E.R. Plummer, R.J. Edmondson, N. J. Curtin, Therapeutic potential of poly(ADP-ribose) polymerase inhibitor AG014699 in human cancers with mutated or methylated BRCA1 or BRCA2, J. Natl. Cancer Inst. 103 (2011) 334–346.
[24] N.S. Cutshall, C. O'Day, M. Prezhdo, Rhodanine derivatives as inhibitors of JSP-1, Bioorg. Med. Chem. Lett. 15 (14) (2005) 3374–3379.
[25] P.H. Carter, P.A. Scherle, J.K. Muckelbauer, M.E. Voss, R.Q. Liu, L.A. Thompson, A. J. Tebben, K.A. Solomon, Y.C. Lo, Z. Li, P. Strzemienski, G. Yang, N. Falahatpisheh, M. Xu, Z. Wu, N.A. Farrow, K. Ramnarayan, J. Wang, D. Rideout, V. Yalamoori, P. Domaille, D.J. Underwood, J.M. Trzaskos, S.M. Friedman, R.C. Newton, C. P. Decicco, Photochemically enhanced binding of small molecules to the tumor necrosis factor receptor-1 inhibits the binding of TNF-α, Proc. Natl. Acad. Sci. U.S. A. 98 (26) (2001) 11879–11884.
[26] R. Dayam, F. Aiello, J. Deng, Y. Wu, A. Garofalo, X. Chen, N. Neamati, Discovery of small molecule integrin $\alpha_v\beta_3$ antagonists as novel anticancer agents, J. Med. Chem. 49 (15) (2006) 4526–4534.
[27] F. Yang, S. Peng, Y. Li, L. Su, Y. Peng, J. Wu, H. Chen, M. Liu, Z. Yi, Y. Chen, A hybrid of thiazolidinone with the hydroxamate scaffold for developing novel histone deacetylase inhibitors with antitumor activities, Org. Biomol. Chem. 14 (5) (2016) 1727–1735.
[28] A. Geronikaki, P. Eleftheriou, P. Vicini, I. Alam, A. Dixit, A.K. Saxena, 2-Thiazolylimino/Heteroarylimino-5-Arylidene-4-Thiazolidinones as new agents with SHP-2 inhibitory action, J. Med. Chem. 51 (17) (2008) 5221–5228.
[29] A. Degterev, A. Lugovskoy, M. Cardone, B. Mulley, G. Wagner, T. Mitchison, J. Yuan, Identification of small-molecule inhibitors of interaction between the BH3 domain and bcl-XL, Nat. Cell Biol. 3 (2) (2001) 173–182.
[30] O. Devinyak, B. Zimenkovsky, R. Lesyk, Biologically active 4-thiazolidinones: a review of QSAR studies and QSAR modeling of antitumor activity, Curr. Top. Med. Chem. 12 (24) (2012) 2763–2784.
[31] A. Verma, S.K. Saraf, 4-Thiazolidinone - a biologically active scaffold, Eur. J. Med. Chem. 43 (5) (2008) 897–905.
[32] A.C. Tripathi, S.J. Gupta, G.N. Fatima, P.K. Sonar, A. Verma, S.K. Saraf, 4-Thiazolidinones: the advances continue, Eur. J. Med. Chem. 72 (2014) 52–77.
[33] A.K. Jain, A. Vaidya, V. Ravichandran, S.K. Kashaw, R.K. Agrawal, Recent developments and biological activities of thiazolidinone derivatives: a review, Bioorg. Med. Chem. 20 (11) (2012) 3378–3395.
[34] K. Appalanaidu, R. Kotcherlakota, T.L. Dadmal, V.S. Bollu, R.M. Kumbhare, C. R. Patra, Synthesis and biological evaluation of novel 2-imino-4-thiazolidinone derivatives as potent anti-cancer agents, Bioorg. Med. Chem. Lett. 26 (21) (2016) 5361–5368.
[35] G. Revelant, S. Huber-Villaume, S. Dunand, G. Kirsch, H. Schohn, S. Hesse, Synthesis and biological evaluation of novel 2-heteroarylimino-1,3-thiazolidin-4-ones as potential anti-tumor agents, Eur. J. Med. Chem. 94 (2015) 102–112.
[36] D.K. Sigalapalli, V. Pooladanda, P. Singh, M. Kadagathur, S.D. Guggilapu, J. L. Uppu, N.D. Tangellamudi, P.K. Gangireddy, C. Godugu, N.B. Bathini, Discovery of certain benzyl/phenethyl thiazolidinone-indole hybrids as potential anti-proliferative agents: synthesis, molecular modeling and tubulin polymerization inhibition study, Bioorg. Chem. 92 (2019) 103188.
[37] D.K. Sigalapalli, V. Pooladanda, M. Kadagathur, S.D. Guggilapu, J.L. Uppu, C. Godugu, N.B. Bathini, N.D. Tangellamudi, Novel chromenyl-based 2-imino-thiazolidin-4-one derivatives as tubulin polymerization inhibitors: design, synthesis, biological evaluation and molecular modelling studies, J. Mol. Struct. 1225 (2021), 128847.
[38] D.K. Sigalapalli, G. Kiranmai, R. Tokala, C. Tripura, R. Ambatwar, S.N. Nunewar, M. Kadagathur, N. Shankaraiah, N. Nagesh, B.N. Babu, N.D. Tangellamudi, Targeting tubulin polymerization and DNA binding of 4-thiazolidinone–umbelliferone hybrids: synthesis and cytotoxicity evaluation, New J. Chem. 45 (40) (2021) 18908–18923.
[39] K.A. Szychowski, M.L. Leja, D.V. Kaminskyy, U.E. Binduga, O.R. Pinyazhko, R. B. Lesyk, J. Gmiński, Study of novel anticancer 4-thiazolidinone derivatives, Chem. Biol. Interact. 262 (2017) 46–56.
[40] L. Zhou, Y. Zhong, M.Z. Xue, D. Kuang, X.W. Cao, Z.J. Zhao, H.L. Li, Y.F. Xu, R. Wang, Design, synthesis and evaluation of PPAR gamma binding activity of 2-thioxo-4-thiazolidinone derivatives, Chin. Chem. Lett. 26 (1) (2015) 63–68.
[41] V. Sriraman, D. Denis, D. De Matos, H. Yu, S. Palmer, S. Nataraja, Investigation of a thiazolidinone derivative as an allosteric modulator of follicle stimulating hormone receptor: evidence for its ability to support follicular development and ovulation, Biochem. Pharmacol. 89 (2) (2014) 266–275.
[42] J. Wrobel, J. Jetter, W. Kao, J. Rogers, L. Di, J. Chi, M.C. Peréz, G.C. Chen, E. S. Shen, 5-Alkylated thiazolidinones as follicle-stimulating hormone (FSH) receptor agonists, Bioorg. Med. Chem. 14 (16) (2006) 5729–5741.
[43] T. Ma, J.R. Thiagarajah, H. Yang, N.D. Sonawane, C. Folli, L.J.V. Galietta, A. S. Verkman, Thiazolidinone CFTR inhibitor identified by high-throughput screening blocks cholera toxin-induced intestinal fluid secretion, J. Clin. Invest. 110 (11) (2002) 1651–1658.
[44] A. Taddei, C. Folli, O. Zegarra-moran, P. Fanen, A.S. Verkman, L.J.V. Galietta, Altered channel gating mechanism for CFTR inhibition by a high-affinity thiazolidinone blocker, FEBS Lett. 558 (1–3) (2004) 52–56.
[45] B. Šarkanj, M. Molnar, M. Čačić, L. Gille, 4-Methyl-7-Hydroxycoumarin antifungal and antioxidant activity enhancement by substitution with thiosemicarbazide and thiazolidinone moieties, Food Chem. 139 (1–4) (2013) 488–495.
[46] M. Čačić, M. Molnar, B. Šarkanj, E. Has-Schön, V. Rajković, Synthesis and antioxidant activity of some new coumarinyl-1,3-thiazolidine- 4-ones, Molecules 15 (10) (2010) 6795–6809.
[47] M.H. Shih, F.Y. Ke, Syntheses and evaluation of antioxidant activity of sydnonyl substituted thiazolidinone and thiazoline derivatives, Bioorg. Med. Chem. 12 (17) (2004) 4633–4643.
[48] R. Tokala, S. Thatikonda, U.S. Vanteddu, S. Sana, C. Godugu, N. Shankaraiah, Design and synthesis of DNA-interactive β-carboline–oxindole hybrids as cytotoxic and apoptosis-inducing agents, ChemMedChem 13 (18) (2018) 1909–1922.
[49] R. Tokala, S. Sana, U.J. Lakshmi, P. Sankarana, D.K. Sigalapalli, N. Gadewal, J. Kode, N. Shankaraiah, Design and synthesis of thiadiazolo-carboxamide bridged β-carboline-indole hybrids: DNA intercalative topo-IIα inhibition with promising antiproliferative activity, Bioorg. Chem. 105 (2020), 104357.
[50] N.D. Tangellamudi, S.B. Shinde, V. Pooladanda, C. Godugu, S. Balasubramanian, Facile synthesis of 2-aryl 5-hydroxy benzo[*d*]Oxazoles and their in vitro anti-proliferative effects on various cancer cell lines, Bioorg. Med. Chem. Lett. 28 (23–24) (2018) 3639–3647.
[51] V. Sharma, T.A. Lansdell, G. Jin, J.J. Tepe, Inhibition of cytokine production by hymenialdisine derivatives, J. Med. Chem. 47 (14) (2004) 3700–3703.
[52] A. Saraste, K. Pulkki, Morphologic and biochemical hallmarks of apoptosis, Cardiovasc. Res. 45 (3) (2000) 528–537.
[53] B. Chazotte, Labeling nuclear DNA using DAPI, Cold Spring Harb. Protoc. 2011 (1) (2011) pdb.prot5556.

[54] D. Ribble, N.B. Goldstein, D.A. Norris, Y.G. Shellman, A simple technique for quantifying apoptosis in 96-well plates, BMC Biotechnol. 5 (2005) 1–7.
[55] M.L. Circu, T.Y. Aw, Reactive oxygen species, cellular redox systems, and apoptosis, Free Radic. Biol. Med. 48 (6) (2010) 749–762.
[56] L.G. Rodriguez, X. Wu, J.L. Guan, Wound-healing assay, Methods Mol. Biol. 294 (2005) 23–29.
[57] a) H. Rafehi, C. Orlowski, G.T. Georgiadis, K. Ververis, A. El-Osta, T. C. Karagiannis, Clonogenic assay: adherent cells, JoVE 49 (2011) 1–4;
b) M. Eray, M. Mattö, M. Kaartinen, L.C. Andersson, J. Pelkonen, Flow cytometric analysis of apoptotic subpopulations with a combination of annexin V-FITC, Propidium iodide, and SYTO 17, Cytometry 43 (2001) 134–142.
[58] S. Satyanarayana, J.C. Dabrowiak, J.B. Chaires, Tris(Phenanthroline) ruthenium (II) enantiomer interactions with DNA: mode and specificity of binding, Biochemistry 32 (10) (1993) 2573–2584.
[59] B. dui Wang, Z.Y. Yang, P. Crewdson, D. qi Wang, Synthesis, crystal structure and DNA-binding studies of the ln(III) complex with 6-hydroxychromone-3-carbaldehyde benzoyl hydrazone, J. Inorg. Biochem. 101 (10) (2007) 1492–1504.
[60] A. Kellett, Z. Molphy, C. Slator, V. McKee, N.P. Farrell, Molecular methods for assessment of non-covalent metallodrug-DNA interactions, Chem. Soc. Rev. 48 (2019) 971–988.
[61] D.K. Jangir, S. Charak, R. Mehrotra, S. Kundu, FTIR and circular dichroism spectroscopic study of interaction of 5-fluorouracil with DNA, J. Photochem. Photobiol. B Biol. 105 (2) (2011) 143–148.
[62] W. Zhong, J.S. Yu, Y. Liang, K. Fan, L. Lai, Chlorobenzylidine-calf thymus DNA interaction II: circular dichroism and nuclear magnetic resonance studies, Spectrochim. Acta Part A Mol. Biomol. Spectrosc. 60 (13) (2004) 2985–2992.
[63] E. Nyarko, N. Hanada, A. Habib, M. Tabata, Fluorescence and phosphorescence spectra of Au(III), Pt(II) and Pd(II) porphyrins with DNA at room temperature, Inorg. Chim. Acta. 357 (3) (2004) 739–745.
[64] H. Fukuda, M. Katahira, N. Tsuchiya, Y. Enokizono, T. Sugimura, M. Nagao, H. Nakagama, Unfolding of quadruplex structure in the G-rich strand of the minisatellite repeat by the binding protein UP1, Proc. Natl. Acad. Sci. U.S.A. 99 (20) (2002) 12685–12690.
[65] J.M. Kelly, A.B. Tossi, D.J. McConnell, C. OhUigin, A study of the interactions of some polypyridylrutheniumn(I) complexes with DNA using fluorescence spectroscopy, topoisomerisation and thermal denaturation, Nucleic Acids Res. 13 (17) (1985) 6017–6034.
[66] J.E. Deweese, M.A. Osheroff, N. Osheroff, DNA topology and topoisomerases: teaching A "knotty" subject, Biochem. Mol. Biol. Educ. 37 (1) (2009) 2–10.
[67] J.L. Nitiss, W.T. Beck, Antitopoisomerase drug action and resistance, Eur. J. Cancer 32A (6) (1996) 958–966.
[68] Y. Pommier, E. Leo, H.L. Zhang, DNA topoisomerases and their poisoning by anticancer and antibacterial drugs, Chem. Biol. 17 (2010) 421–433.
[69] Schrödinger Release 2017-1, Maestro, Schrödinger, LLC, New York, NY, 2017.
[70] B.L. Staker, K. Hjerrild, M.D. Feese, C.A. Behnke, A.B. Burgin, L. Stewart, The mechanism of topoisomerase I poisoning by a camptothecin analog, Proc. Natl. Acad. Sci. U.S.A. 99 (24) (2002) 15387–15392.
[71] Version 5.1, Qikprop, Schrödinger, LLC, New York, NY, 2017.
[72] K. Enslein, V.K. Gombar, B.W. Blake, International commission for protection against environmental mutagens and carcinogens. Use of SAR in computer-assisted prediction of carcinogenicity and mutagenicity of chemicals by the TOPKAT program, Mutat. Res. 305 (1994) 47–61.
[73] J. Dearden, *In silico* prediction of drug toxicity, J. Comput. Aided Mol. Des. 17 (2003) 119–127.
[74] C. Tan, J. Liu, L. Chen, S. Shi, L. Ji, Synthesis, structural characteristics, DNA binding properties and cytotoxicity studies of a series of Ru(III) complexes, J. Inorg. Biochem. 102 (8) (2008) 1644–1653.
[75] T.S. Dexheimer, Y. Pommier, DNA cleavage assay for the identification of topoisomerase I inhibitors, Nat. Protoc. 3 (11) (2008) 1736–1750.
[76] A. Siwek, A. Bielawska, E. Maciorkowska, M. Lepiarczyk, K. Bielawski, N. Trotsko, M. Wujec, Cytotoxicity and topoisomerase I/II inhibition activity of novel 4-Aryl/alkyl-1-(piperidin-4-yl)-carbonylthiosemicarbazides and 4-benzoylthiosemicarbazides, J. Enzym. Inhib. Med. Chem. 29 (2) (2014) 243–248.
[77] A. Negi, J.M. Alex, S.M. Amrutkar, A.T. Baviskar, G. Joshi, S. Singh, U.C. Banerjee, R. Kumar, Imine/amide–imidazole conjugates derived from 5-Amino-4-cyano-N1-substituted benzyl imidazole: microwave-assisted synthesis and anticancer activity *via* selective topoisomerase-IIα inhibition, Bioorg. Med. Chem. 23 (2015) 5654–5661.